Rab27a controls HIV-1 assembly by regulating plasma membrane levels of phosphatidylinositol 4,5-bisphosphate

Pehuén Pereyra Gerber,[1]* Mercedes Cabrini,[1]* Carolina Jancic,[2] Luciana Paoletti,[3] Claudia Banchio,[3] Catalina von Bilderling,[4] Lorena Sigaut,[5] Lía I. Pietrasanta,[5] Gabriel Duette,[1] Eric O. Freed,[6] Genevieve de Saint Basile,[7,8] Catarina Ferreira Moita,[9] Luis Ferreira Moita,[9] Sebastian Amigorena,[10] Philippe Benaroch,[10] Jorge Geffner,[1] and Matías Ostrowski[1]

[1]Instituto de Investigaciones Biomédicas en Retrovirus y Síndrome de Inmunodeficiencia Adquirida (INBIRS)–Consejo Nacional de Investigaciones Científicas y Técnicas (CONICET), Universidad de Buenos Aires, C1121ABG Buenos Aires, Argentina
[2]Instituto de Medicina Experimental–CONICET, Academia Nacional de Medicina, C1425AUM Buenos Aires, Argentina
[3]Instituto de Biologia Molecular y Celular de Rosario–CONICET, S2000EZP Santa Fe, Argentina
[4]Instituto de Física de Buenos Aires–CONICET, Departamento de Física; and [5]Centro de Microscopías Avanzadas; Facultad de Ciencias Exactas y Naturales, Universidad de Buenos Aires, C1428EGA Buenos Aires, Argentina
[6]Virus–Cell Interaction Section, HIV Drug Resistance Program, National Cancer Institute, Frederick, MD 21702
[7]Institut National de la Santé et de la Recherche Médicale U768 and [8]Institut Imagine, Université Paris Descartes-Sorbonne Paris Cité, 75015 Paris, France
[9]Innate Immunity and Inflammation Laboratory, Instituto Gulbenkian de Ciencia, 2780-156 Oeiras, Portugal
[10]Centre de Recherche, Institut National de la Santé et de la Recherche Médicale U932, Institut Curie, 75248 Paris, France

During the late stages of the HIV-1 replication cycle, the viral polyprotein $Pr55^{Gag}$ is recruited to the plasma membrane (PM), where it binds phosphatidylinositol 4,5-bisphosphate ($PI(4,5)P_2$) and directs HIV-1 assembly. We show that Rab27a controls the trafficking of late endosomes carrying phosphatidylinositol 4-kinase type 2 α (PI4KIIα) toward the PM of $CD4^+$ T cells. Hence, Rab27a promotes high levels of PM phosphatidylinositol 4-phosphate and the localized production of $PI(4,5)P_2$, therefore controlling $Pr55^{Gag}$ membrane association. Rab27a also controls $PI(4,5)P_2$ levels at the virus-containing compartments of macrophages. By screening Rab27a effectors, we identified that Slp2a, Slp3, and Slac2b are required for the association of $Pr55^{Gag}$ with the PM and that Slp2a cooperates with Rab27a in the recruitment of PI4KIIα to the PM. We conclude that by directing the trafficking of PI4KIIα-positive endosomes toward the PM, Rab27a controls $PI(4,5)P_2$ production and, consequently, HIV-1 replication.

Introduction

Productive HIV assembly requires the coordinated mobilization of both viral and cellular host factors toward the plasma membrane (PM) domains where formation of viral particles takes place. This process is orchestrated by the viral precursor protein $Pr55^{Gag}$, a myristoylated polyprotein that contains four major structural domains: matrix, capsid, nucleocapsid, and p6. A highly basic region present in the matrix domain is responsible for binding to phosphatidylinositol 4,5-bisphosphate ($PI(4,5)P_2$), a phosphoinositide present at the inner leaflet of the PM. Upon binding $PI(4,5)P_2$, $Pr55^{Gag}$ molecules multimerize and form a spherical shell that packages the genomic RNA into the nascent virion. Concomitantly, the viral envelope protein Env is recruited and incorporated into the nascent viral particles. During virus release, the viral protease cleaves $Pr55^{Gag}$ into its constituent

*P.P. Gerber and M. Cabrini contributed equally to this paper.

Correspondence to Matías Ostrowski: maostro@fmed.uba.ar

Abbreviations used in this paper: CMV, cytomegalovirus; Ct, cycle threshold; DIC, differential interference contrast; fps, frames per second; GM-CSF, granulocyte–macrophage colony-stimulating factor; GS, Griscelli syndrome; LRO, lysosome-related organelle; LSCM, laser-scanning confocal microscopy; MDM, monocyte-derived macrophage; MVEs, multivesicular endosomes; PBMC, peripheral blood mononuclear cell; PE, phycoerythrin; PH, pleckstrin homology; p.i., postinfection; $PI(4,5)P_2$, phosphatidylinositol 4,5-bisphosphate; PI(4)P, phosphatidylinositol 4-phosphate; PM, plasma membrane; qPCR, quantitative RT-PCR; TEMs, tetraspanin-enriched microdomains; TLC, thin layer chromatography; VCCs, virus-containing compartments.

The Rockefeller University Press $30.00
J. Cell Biol. Vol. 209 No. 3 435–452
www.jcb.org/cgi/doi/10.1083/jcb.201409082

proteins, giving rise to mature infectious viral particles (Balasubramaniam and Freed, 2011; Sundquist and Kräusslich, 2012). Whereas in CD4+ T cells, HIV-1 assembles at discrete domains of the PM, in macrophages, HIV-1 budding takes place in specialized, intracellular sequestered portions of the PM known as virus-containing compartments (VCCs; Deneka et al., 2007; Jouve et al., 2007; Welsch et al., 2007; Bennett et al., 2009; Benaroch et al., 2010). In both cases, the HIV-1 assembly domains present a peculiar enrichment for a variety of tetraspanins, such as CD9, CD63, CD81, and CD82 (Booth et al., 2006; Deneka et al., 2007; Jolly et al., 2011). However, the role played by tetraspanins at the site of HIV-1 assembly still remains an open question in the field.

The trafficking of late endosomes/secretory lysosome toward the site of HIV-1 assembly has been shown to be required for the dissemination of HIV-1 infection in CD4+ T cells (Jolly et al., 2011). Indeed, cells isolated from Chediak–Higashi and Hermansky–Pudlack syndrome patients, two rare autosomal recessive diseases that affect late endosomes/lysosomes, are deficient in HIV-1 production (Dong et al., 2005; Jolly and Sattentau, 2007). Moreover, several cellular proteins implicated in endosomal function have been shown to be required for $Pr55^{Gag}$ trafficking (Balasubramaniam and Freed, 2011). Along these lines, it has been proposed that during viral assembly and release, HIV-1 hijacks the cellular exosome secretion pathway (Gould et al., 2003; Booth et al., 2006). Exosome secretion takes place after the fusion of the limiting membrane of multivesicular endosomes (MVEs) with the PM, resulting in the extracellular release of their intraluminal vesicles, which are then named as exosomes (Théry et al., 2009). We previously showed that small GTPases Rab27a and Rab27b control exosome secretion by promoting the docking of MVEs to the PM (Ostrowski et al., 2010). Taking into consideration the role played by Rab27a in regulating the trafficking of late endosomes and exosome secretion and the proposed link between these processes and HIV-1 assembly, in this study, we undertook the analysis of the role played by late endosomal compartments in HIV-1 budding by using cells deficient in Rab27a.

We show that Rab27a controls the recruitment of PI4KIIα (phosphatidylinositol 4-kinase type 2 α) from endosomes to the PM, promoting high levels of phosphatidylinositol 4-phosphate (PI(4)P) and fueling $PI(4,5)P_2$ production. This, in turn, favors the recruitment of $Pr55^{Gag}$ and HIV-1 assembly. We also show that Rab27a uses its effector Slp2a to promote PI4KIIα recruitment and the production of PI(4)P and PI(4,5)P2 at the PM. In summary, our study identifies a Rab27a-controlled endosomal trafficking pathway usurped by HIV-1 during viral assembly.

Results

Silencing of Rab27a inhibits HIV-1 replication in CD4+ T cells and macrophages

The role of Rab27a in HIV-1 replication was first analyzed by silencing the expression of this small GTPase in the CD4+ T cell line Jurkat by using two different Rab27a shRNA sequences (Fig. 1 A). Upon infection with a VSV-G–pseudotyped HIV-1 strain, which circumvents the viral receptors and enters the cells through endocytosis (Naldini et al., 1996), the two Rab27a shRNA sequences significantly impaired HIV-1 replication, as determined by reduced production of p24 antigen at day 5 postinfection (p.i.; Fig. 1 B). Given that the strongest effect on Rab27a mRNA silencing was observed with shRNA sequence #2, this construct was chosen for the next set of experiments. The ability of shRNA#2 to silence Rab27a expression was confirmed by immunoblotting (Fig. 1 C). The percentage of live cells in control and Rab27a-silenced cells, evaluated by Annexin V/propidium iodide staining, showed that Rab27a silencing did not affect cell viability (Fig. 1 D). To rule out off-target effects of the shRNA treatment, we rescued Rab27a expression in Rab27a-silenced cells and observed a reversion of the inhibition in HIV-1 replication (Fig. S1, A and B), confirming the specificity of the results.

The kinetics of HIV-1 production was then evaluated by infecting Jurkat cells with a CXCR4-tropic HIV-1 strain (IIIb) at a low MOI. In these experimental conditions, HIV-1 replication in Rab27a-silenced cells was also severely impaired (Fig. 1, E, F, and G).

Further experiments were performed to assess whether Rab27a was required for early or late stages of the viral replication cycle. The lack of differences between control and Rab27a-silenced cells in (a) cell surface levels of CD4 and CXCR4 (HIV-1 receptor and coreceptor, respectively; Fig. S2 A), (b) the amount of HIV-1 attached to the cell surface (measured after coincubating cells and virus at 4°C for 90 min) and internalized (measured after coincubating cells and virus at 37°C; Fig. S2 B), and (c) the susceptibility to HIV-1 infection in a single-cycle assay (Fig. S2, C and D) allowed us to conclude that Rab27a does not interfere with early steps of the HIV-1 replication cycle. To analyze the role of Rab27a in the late stages of the viral replication cycle, cells were spinoculated with HIV-1 at a high MOI to achieve a high percentage of infected cells at 48 h p.i. The amount of cell-associated $Pr55^{Gag}$ in control and Rab27a-silenced cells was similar, showing that, as in the case of wild-type HIV-1, the entry of VSV-G–pseudotyped viral particles is not affected in Rab27a-silenced cells (Fig. 1 H, left). However, the amount of virus released into the supernatant was dramatically reduced in Rab27a-silenced cells (Fig. 1 H, right), suggesting that the inhibition of HIV-1 replication observed in Rab27a-silenced cells is mainly caused by a defect in the assembly or release of viral particles. Taking into consideration that the host restriction factor tetherin inhibits HIV-1 release, we next decided to analyze whether Rab27a expression modified tetherin surface expression. Both in uninfected and in HIV-1–infected cells, tetherin expression in Rab27a-silenced cells was comparable to that of control cells (Fig. S2, E–H). Thus, silencing the expression of Rab27a impairs HIV-1 replication by controlling a tetherin-independent late step of the viral replication cycle.

We then analyzed the role of Rab27a in HIV-1 replication in primary CD4+ T cells by using two strategies. First, expression of Rab27a was silenced by transducing peripheral blood mononuclear cells (PBMCs) with Rab27a shRNA#2 (efficiency of silencing: 52%). In addition, PBMCs from a patient with a mutation in Rab27a, a clinical condition known as Griscelli syndrome (GS; Ménasché et al., 2005), and an age-matched healthy

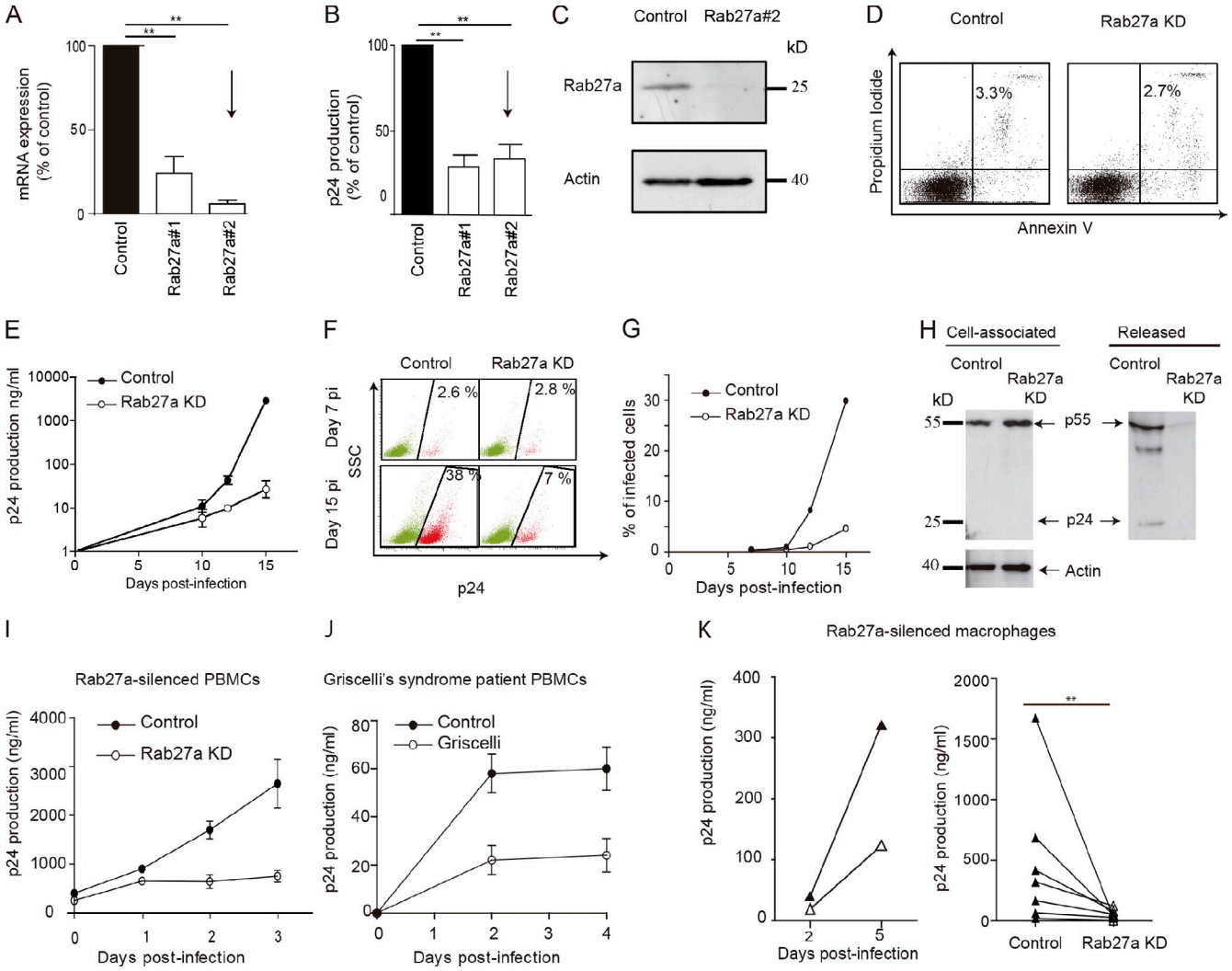

Figure 1. **Rab27a is required for HIV replication in CD4⁺ T lymphocytes and macrophages.** (A–D) Jurkat cells were transduced with lentivirus encoding different Rab27a shRNA sequences (A and B; open bars), or a control scrambled shRNA (black bars). (A) Rab27a mRNA levels were determined by qPCR. Means ± SD of a representative experiment (n = 3) performed in triplicates is shown. (B) Cells (3×10^4/0.1 ml) were infected with a VSV-G–pseudotyped HIV (20 ng p24/ml), and p24 production was evaluated in cell supernatants at day 5 p.i. Means ± SD of two independent experiments expressed as percentages of p24 production of control cells are shown. (C) Immunoblot of Rab27a protein levels. Actin was used as a loading control. (D) Cell viability was determined at day 7 after puromycin selection by annexin V staining and propidium iodide exclusion followed by FACS analysis. Dot plots from a representative experiment (n = 4) are shown. Percentage of death cells (annexin V⁺/propidium iodide⁺) is indicated. (E–G) Control (closed circles) and Rab27a-silenced Jurkat cells (open circles; 3×10^4/0.1 ml) were infected with HIV (IIIb strain; 50 ng p24/ml). The production of p24 (E) and the percentages of p24-positive cells (F and G) were determined by ELISA and FACS analysis, respectively. Representative dot plots (F) and the percentages of infected cells (G) from a representative experiment (n = 6) are shown. (H) Virus release assay. Cells were spinoculated with a high MOI of VSV-G–pseudotyped HIV strain. 48 h later, the amounts of cell-associated and released virus were analyzed by immunoblotting. (I and J) Control and Rab27a-silenced PBMCs (I) or PBMCs from a GS patient and an age-matched control (J) were infected with a VSV-G–pseudotyped HIV-1 (200 and 50 ng/ml p24, respectively). The production of p24 was evaluated at different days p.i. Results from a representative experiment (n = 3 and n = 2) performed in triplicates are expressed as the means ± SD. (K) Quantification of p24 antigen in cell supernatants from control (closed triangles) or Rab27a-silenced (open triangles) MDMs (5×10^4/0.1 ml) infected with HIV-1(BaL strain; 50 ng p24/ml). Kinetics of p24 production from a representative experiment are shown in the left graph. p24 production by cells from seven different blood donors at day 5 p.i. is shown in the right graph. Asterisks indicate statistically significant differences from the control: **, $P < 0.01$. KD, knockdown.

donor were used. In agreement with results obtained in Jurkat cells, Rab27a-deficient lymphocytes produced significantly less virus, as compared with their respective controls (Fig. 1, I and J). Finally, the role of Rab27a in HIV-1 production was analyzed in primary macrophages. In this case too, we observed that Rab27a silencing (efficiency of silencing: >90%) impaired HIV-1 replication (Fig. 1 K). We conclude that Rab27a is required for a late step of the HIV-1 replication cycle, both in CD4⁺ T cells and monocyte-derived macrophages (MDMs).

Rab27a controls the formation of the HIV-1 assembly platform and Gag recruitment to cell membranes in CD4⁺ T cells and macrophages

Rab27 controls the intracellular trafficking of MVEs (Ostrowski et al., 2010) and of several lysosome-related organelles (LROs) in different cell types (Raposo et al., 2007). To explore whether the impairment of HIV-1 assembly observed in Rab27a-silenced cells was related to a defect in the trafficking of these organelles,

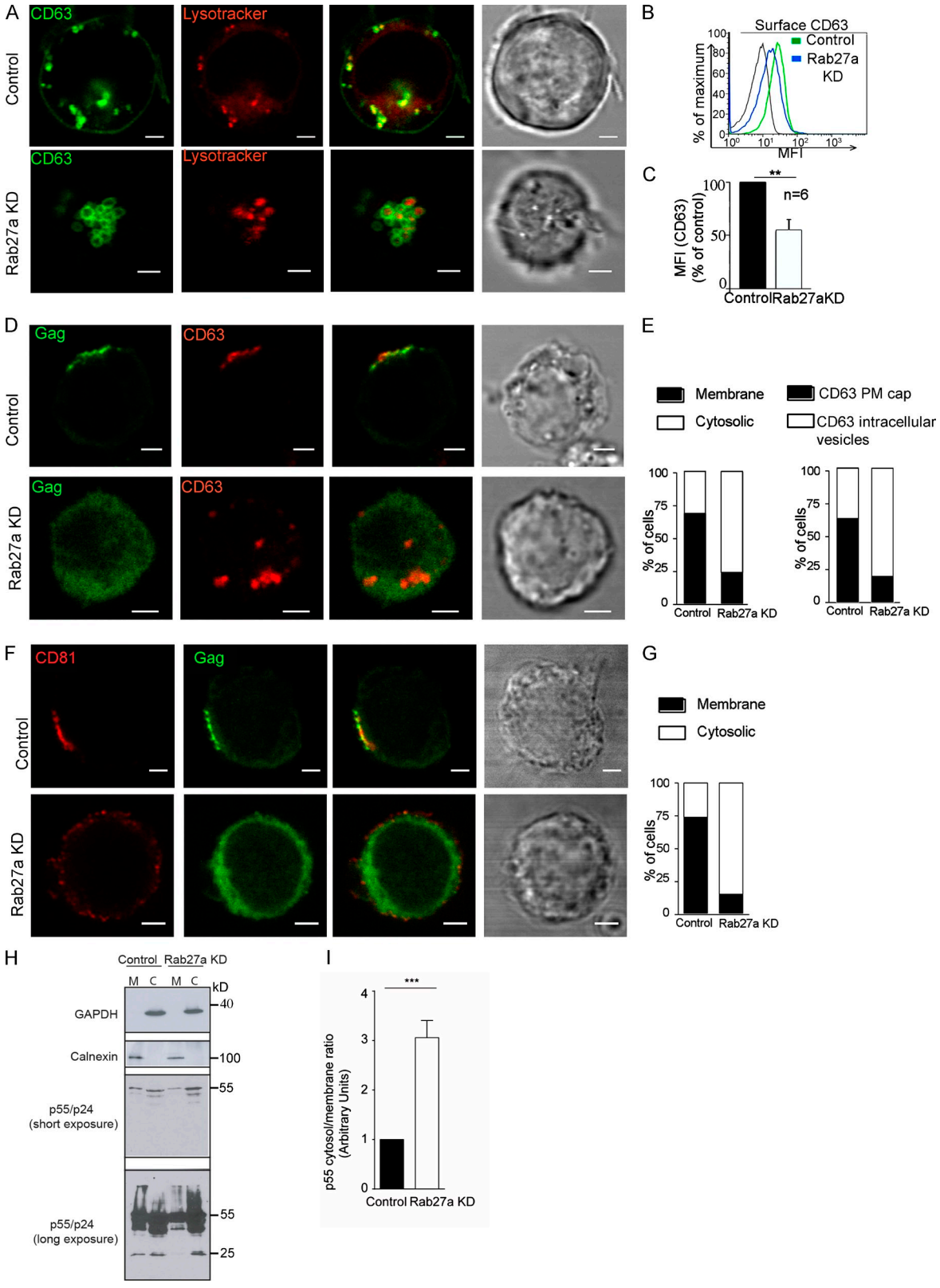

Figure 2. **Silencing of Rab27a impairs the recruitment of MVEs to the site of HIV-1 assembly and Pr55^{Gag} association with the PM in Jurkat cells.** (A) LSCM of live control and Rab27a-silenced cells stably expressing CD63-GFP and stained with LysoTracker. (B) FACS plots showing endogenous cell surface CD63 levels in control and Rab27a-silenced cells. Isotype control is shown (gray line). The data shown are from a single representative experiment out of six repeats. For the experiment shown, 10,000 cells from each condition were analyzed. (C) Mean fluorescence intensity (MFI) of cell surface CD63 staining in control and Rab27a-silenced cells ($n = 6$). (D) Immunofluorescence LSCM images of endogenous CD63 and Gag in control and Rab27a-silenced infected Jurkat cells at day 12 p.i. To better visualize Gag cytosolic distribution in Rab27a-silenced cells, the laser power was increased for the acquisition of the green channel. (E) Quantitation of PM versus cytosolic distribution of Gag and of CD63 forming a PM cap versus its intracellular location in 100 cells of each condition. Data are expressed as percentages of cells in each category. (F) LSCM of control and Rab27a-silenced Jurkat cells. Cell surface CD81

we performed laser-scanning confocal microscopy (LSCM) in live cells using the tetraspanin CD63 and LysoTracker (a dye that labels acidic compartments) as markers of LRO/endosome identity. Rab27a-silenced cells presented a marked increase in the size of GFP-CD63$^+$ compartments concomitantly with a reduction in the amount of PM-associated CD63, as compared with control cells (Fig. 2 A). This phenotype could be reverted by the expression of exogenous Rab27a (Fig. S3, A and B). The reduction in PM levels of endogenous CD63 was also indicated by FACS analysis (Fig. 2, B and C). To further analyze whether the reduction in PM levels of CD63 in Rab27a-silenced cells was caused by a defect in the trafficking of CD63$^+$ endosomes, we performed a CD4$^+$ T cell degranulation assay based on the quantification of CD63 cell surface translocation after stimulation of the cells with PMA-ionomycin. Translocation of CD63 from internal compartments to the PM was severely impaired in Rab27a-silenced cells (Fig. S3, C and D), suggesting that the Rab27a-regulated pathway of endosomal trafficking significantly contributes to PM levels of CD63. To rule out an effect of Rab27a on the functionality of the regular secretory pathway, the secretion of the cytokine granulocyte–macrophage colony-stimulating factor (GM-CSF; that follows the conventional secretory pathway) was assessed by ELISA. No changes in the secretion of this cytokine were observed (Fig. S3 E), confirming previous results showing that Rab27a does not interfere with the regular secretory pathway of the cell (Ostrowski et al., 2010). Altogether, these results suggest that by controlling the trafficking of CD63-positive endosomes/LROs, Rab27a promotes PM localization of CD63 in CD4$^+$ T cells.

We next analyzed the Rab27a-mediated trafficking of CD63$^+$ endosomes in HIV-1–infected cells by LSCM immunofluorescence analysis. In agreement with a previous study (Jolly et al., 2011), we observed that in HIV-1–infected control cells, CD63 was redistributed from its predominantly internal localization toward a discrete, polarized domain of the PM, where it showed a high level of colocalization with Gag (Fig. 2 D). In contrast, in Rab27a-silenced cells, CD63$^+$ endosomes remained scattered throughout the cytoplasm and the formation of a PM cap of CD63 was not observed. This alteration in endosomal trafficking was concomitant with a change in Gag distribution, which instead of being predominantly associated with the PM, acquired a cytosolic distribution. (Fig. 2, D and E). These changes were not caused by alterations in the production of Pr55^{Gag}, as revealed by analysis of the mean fluorescence intensity of Pr55^{Gag} staining by FACS (mean fluorescence intensity of control cells = 5,848 ± 215 vs. 5,695 ± 197 in Rab27a-silenced cells).

In addition to containing high levels of CD63, the site of HIV-1 assembly also presents an important enrichment in CD81 (Jolly and Sattentau, 2007; Krementsov et al., 2009), another tetraspanin that, unlike CD63, is exclusively present at the PM of Jurkat cells and not in endosomes (Fig. S4 A). LSCM visualization of control cells revealed high levels of colocalization between Pr55^{Gag} and cell surface CD81 in patched regions of the PM (Fig. 2, F and G). In contrast, as mentioned in the previous paragraph, in Rab27a-silenced cells, Gag exhibited a predominantly cytosolic distribution. In addition, despite the fact that CD81 distribution in uninfected Rab27a-silenced CD4$^+$ T cells was comparable to that of control cells (Fig. S4 B), the HIV-1–induced coalescence of CD81 into discrete domains at the PM was inhibited in cells deficient for Rab27a (Fig. 2, F and G). These results suggest that Rab27a is required for the proper targeting of Pr55^{Gag} to the PM and for the reorganization of the tetraspanin-enriched microdomains (TEMs).

The decrease in the association of Pr55^{Gag} with the PM in Rab27a-silenced cells was confirmed by immunoblot analysis of Pr55^{Gag} distribution in cytosolic and membrane fractions (Fig. 2, H and I). Interestingly, the p24 capsid protein was detected in association with cell membranes in control cells (likely representing mature viral particles in the process of budding) but not in Rab27a-silenced cells (Fig. 2 H, longer exposure).

We then decided to analyze Pr55^{Gag} distribution in Rab27a-deficient primary cells. The use of cells from a GS patient recapitulated the phenotype observed in Jurkat cells, further confirming that Rab27a is required for Pr55^{Gag} membrane association (Fig. 3, A and B). Finally, Pr55^{Gag} distribution was analyzed in MDMs. In agreement with previous studies (Raposo et al., 2002; Ono et al., 2004; Deneka et al., 2007), we found that in control MDMs, Gag was noticeably concentrated in discrete apparently intracellular compartments, usually identified as VCCs, showing a high degree of colocalization with CD81 (Fig. 3 C, top). In contrast, in Rab27a-silenced MDMs, Gag exhibited a diffuse, cytosolic staining pattern (Fig. 3, C [bottom] and D).

Rab27a silencing does not disrupt Env trafficking and processing

Whereas Pr55^{Gag} is recruited from the cytosol directly to the HIV-1 assembly site at the PM, Env reaches the PM through the regular ER–Golgi-dependent secretory pathway (Checkley et al., 2011). To rule out an effect of Rab27a in Env trafficking, the expression of total and cell surface Env was determined by FACS analysis in Jurkat cells at day 10 p.i. Consistent with the defect in HIV-1 replication shown in Fig. 1, the percentage of HIV-infected (Env positive) cells was lower in Rab27a-silenced cells (Fig. 4, A and B). However, the mean fluorescence intensity of both total and cell surface Env in infected cells was similar in both conditions (Fig. 4, A and B), indicating that Env expression and trafficking to the PM were not perturbed

was stained in nonpermeabilized cells, and, subsequently, intracellular Gag was stained. (G) Quantitation of PM versus cytosolic distribution of Gag was evaluated in 100 cells of each condition. Data are expressed as percentages of cells in each category. (H) Immunoblots of cell fractions to analyze the distribution of Pr55^{Gag} and p24. The purity of the fractions was assessed by detection of the cytosolic protein GAPDH and the membrane-associated protein calnexin. M, membrane fraction; C, cytosolic fraction. One representative experiment out of three is shown. (I) Ratio of cytosol/membrane distribution of p55, corresponding to three independent experiments. In A, D, and F, transmitted light channel is shown on the right. The quantifications shown in E and G were performed by blinded observers on a per cell basis. KD, knockdown. **, $P < 0.01$; ***, $P < 0.001$. Bars, 2 µm.

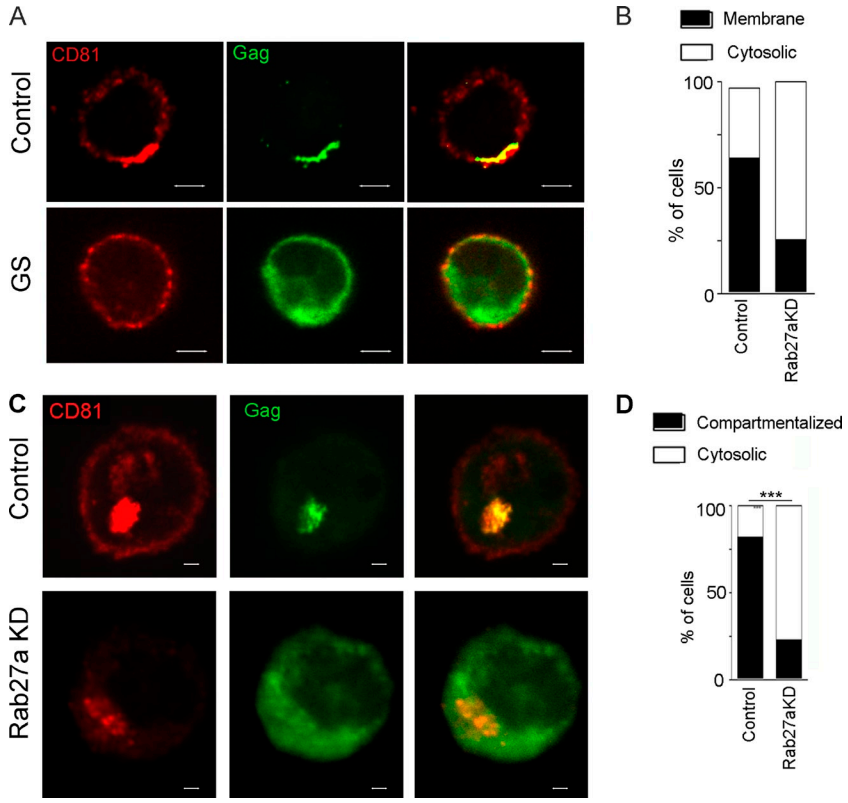

Figure 3. **Rab27a controls Pr55^{Gag} recruitment to cell membranes in CD4$^+$ T cells and macrophages.** (A) 3D deconvolution fluorescence microscopy of HIV-1–infected PBMCs from a healthy control or a GS patient stained at day 4 p.i. with anti-p24 (green) and anti-CD81 antibodies. Shown is a 3D maximum intensity projection of 10 optical sections acquired at 0.2-µm intervals. (B) Quantitation of PM versus cytosolic distribution of Gag was evaluated by blinded observers on a per-cell basis, in 100 cells of each condition. Data are expressed as percentages of cells in each category. (C) LSCM of HIV-1–infected control or Rab27a-silenced MDMs stained at day 5 p.i. with anti-p24 (green) and anti-CD81 antibodies. (D) Quantification of Gag distribution was performed as described in B. ***, $P < 0.001$. KD, knockdown. Bars, 2 µm.

by Rab27a silencing. Indeed, LSCM analysis showed that in both control and Rab27a-silenced cells, Env exhibited a similar distribution, being present both in intracellular compartments and at the PM (Fig. 4 C). Moreover, the proteolytic processing of gp160 by furin or furin-like proteases located in the Golgi (Checkley et al., 2011), evaluated as the ratio of gp41/gp160, was similar in control and Rab27a-silenced cells (Fig. 4, D and E), further indicating that Env processing at the Golgi is not altered upon Rab27a silencing. Finally, the infectivity of the viral particles still produced by Rab27a-silenced cells was assessed by infecting the reporter cell line GHOST with equal amounts of HIV-1 secreted by control and Rab27a-silenced cells. The lack of difference in the infectivity of HIV-1 particles produced by control and Rab27a-silenced cells provided functional evidence supporting the notion that Env incorporation into viral particles was not modified upon Rab27a silencing (Fig. 4 F). Altogether, these results indicate that Rab27a specifically regulates Pr55^{Gag} trafficking without affecting the arrival of Env to the PM.

Formation of virological synapses and cell-to-cell transmission of HIV-1 are inhibited in Rab27a-deficient cells

Direct cell-to-cell transfer of HIV-1 is a more efficient way of propagating the infection, as compared with transmission by cell-free viral particles (Dimitrov et al., 1993; Carr et al., 1999). Our results anticipate that, by preventing Pr55^{Gag} from reaching the PM, silencing of Rab27a will also limit both the amount of Pr55^{Gag} at the virological synapse and cell–cell transfer of HIV-1. Indeed, silencing of Rab27a expression abrogated the polarized distribution of Gag at zones of cell-to-cell contact in Jurkat cells (Fig. 5, A and B). A similar phenotype was observed in primary CD4$^+$ T cells isolated from a GS patient (Fig. 5 C) and in MDMs incubated with autologous activated PBMCs (Fig. 5 D).

To measure cell-to-cell transmission of HIV-1, the percentage of HIV-1–infected control or Rab27a-silenced cells at day 10 p.i. was determined by FACS. Because the percentage of HIV-1–infected cells was higher in control cells than in Rab27a-silenced cells, we normalized the percentage of HIV-1–infected cells in each condition by adding noninfected control cells to cultures of HIV-1–infected control cells to have 6% of HIV-infected cells in a total of 80,000 cells for each condition. (Fig. 5 E, left, donor cells). Cells were then added to cultures of GHOST cells (target), either in direct contact or separated by a filter membrane with pores that allow the passage of HIV-1 particles but not of cells. Silencing Rab27a expression impaired HIV-1 transmission both through cell–cell contact and through free viral particles (Fig. 5 E, right). These results indicate that Rab27a is required for the formation of virological synapses in both MDMs and CD4$^+$ T cells and for HIV-1 cell-to-cell transmission in CD4$^+$ T cells.

Rab27a controls the levels of PI(4,5)P_2 in the PM of CD4$^+$ T cells and in macrophage VCCs

Targeting of Pr55^{Gag} to the PM is directed by PI(4,5)P_2 (Ono et al., 2004). Thus, we sought to investigate whether the reduction in Pr55^{Gag} association with the PM in Rab27a-silenced cells was caused by a reduction in PM levels of PI(4,5)P_2.

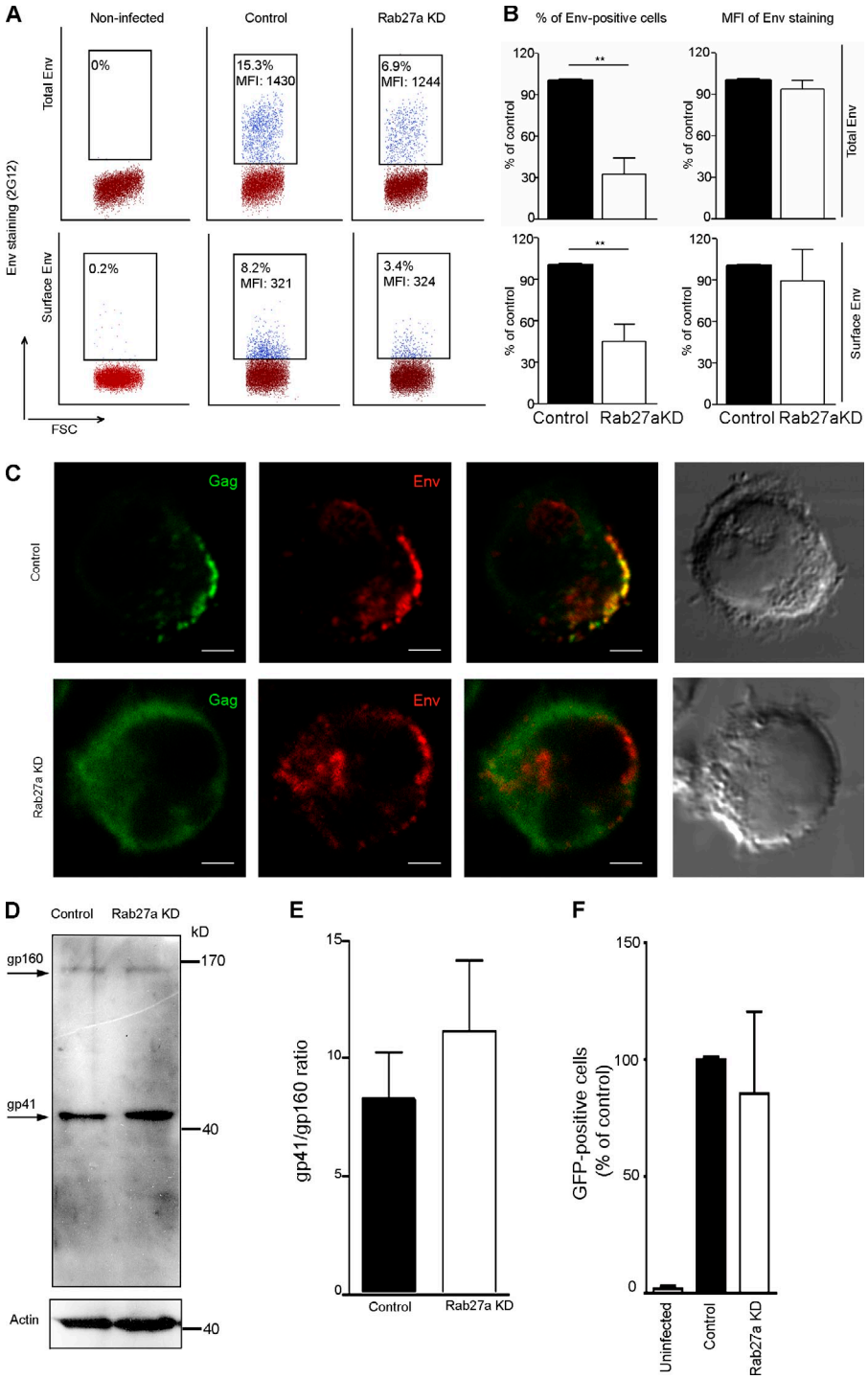

Figure 4. **Rab27a silencing does not disrupt Env trafficking.** Control and Rab27a-silenced cells were infected with HIV (IIIb strain) and analyzed at day 10 p.i. (A) Representative FACS plot showing Total (top) and cell surface (bottom) Env levels in uninfected, control, and Rab27a-silenced cells. The percentage of Env-positive cells in the gate containing Env-positive cells is indicated. (B) Quantification of FACS data from three independent experiments. (C) LSCM of control and Rab27a-silenced Jurkat cells stained with anti-p24 (green) and anti-Env antibodies. Differential interference contrast (DIC) images are shown on the right. Bars, 2 µm. (D) gp41 immunoblot on cells spinoculated with a high MOI of vesicular stomatitis virus–pseudotyped HIV at day 3 p.i. (E) gp41/gp160 ratio in control and Rab27a-silenced cells (n = 2). (F) Infectivity of the virions produced by control and Rab27a-silenced cells was evaluated using the same amount of p24 (10 ng, as determined by ELISA) to infect GHOST cells (n = 3). Results are normalized to the value obtained by infecting GHOST cells with the virus contained in the supernatant of control cells. Error bars show SDs. KD, knockdown; MFI, mean fluorescence intensity. **, P < 0.01. Bars, 2µm.

The intracellular distribution of $PI(4,5)P_2$ was evaluated by LSCM in Jurkat cells transduced with a GFP-tagged pleckstrin homology (PH) domain derived from phospholipase Cδ1 (PH-GFP; Várnai and Balla, 1998). Staining of cell surface CD81 in nonpermeabilized cells was used to better define the localization of the PM. PH-GFP labeling of the PM was considerably reduced in Rab27a-silenced cells (Fig. 6, A–C). To assess global cellular levels of $PI(4,5)P_2$ biochemically, the amount of [^{32}P]orthophosphate incorporated into $PI(4,5)P_2$ molecules was analyzed by thin layer chromatography (TLC; Fig. 6 D), confirming that the amount of [^{32}P]-labeled $PI(4,5)P_2$ was significantly lower in Rab27a-silenced cells (Fig. 6 E). Paralleling the results obtained in Jurkat cells, silencing of Rab27a in primary $CD4^+$ T cells also resulted in a significant loss of PH-GFP staining at the PM (Fig. 6, F and G). Finally, $PI(4,5)P_2$ distribution was analyzed in Rab27a-silenced MDMs. In agreement with previous studies (Mlcochova et al., 2013), in control cells, $PI(4,5)P_2$ was enriched at the PM as well as in intracellular structures, which were also positive for CD81 (Fig. 6 H, top). In contrast, in Rab27a-silenced

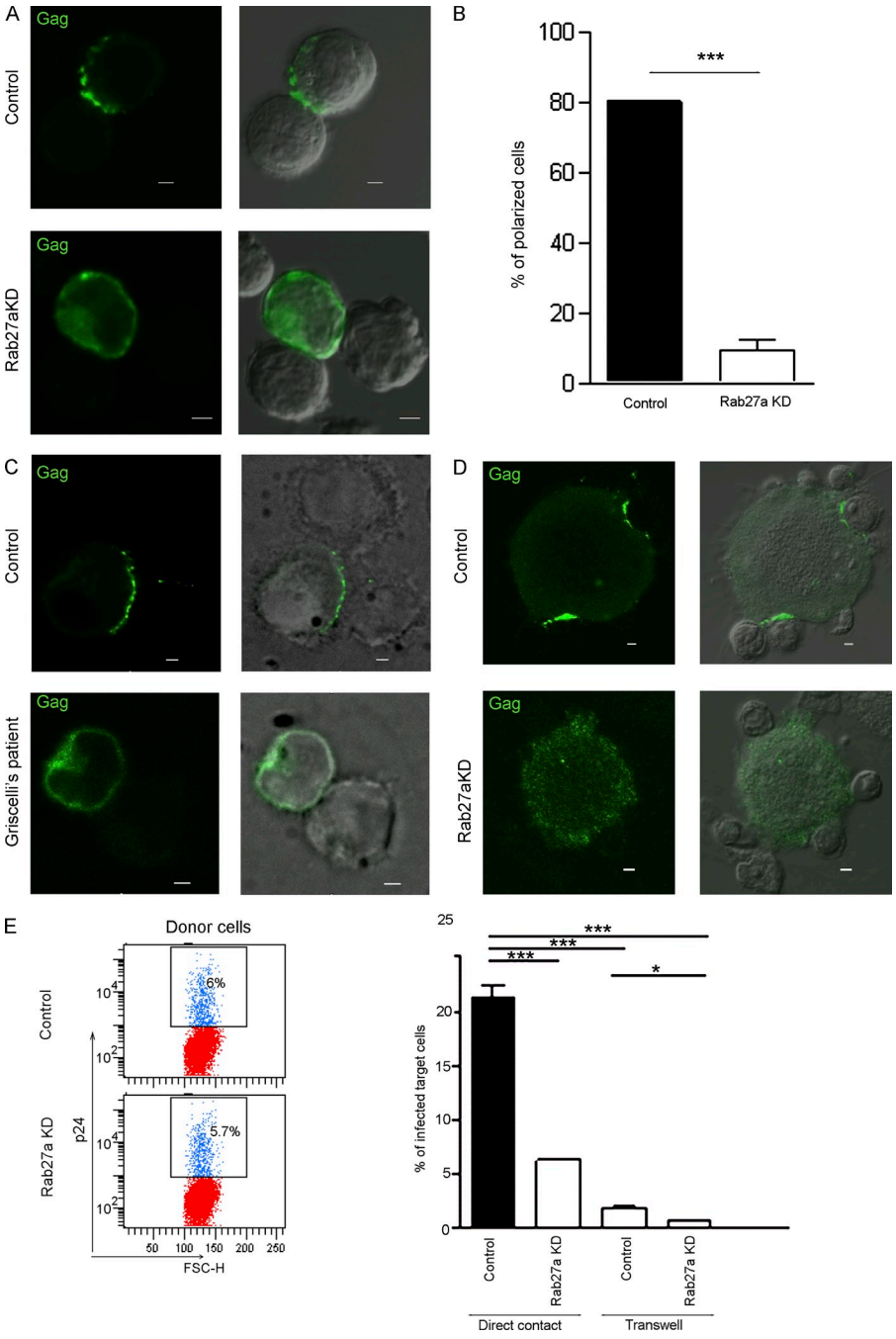

Figure 5. **Formation of the virological synapse and cell-to-cell transmission of HIV are impaired in Rab27a-deficient cells.** (A) Control or Rab27a-silenced Jurkat cells were infected with HIV (IIIB strain). At day 7 p.i., cells were plated onto poly-L-lysine–coated coverslips and incubated with noninfected target Jurkat cells for 1.5 h. Gag was stained with anti-p24 antibodies and polarization of Gag at the virological synapses was evaluated by LSCM. Representative confocal and DIC images are shown. (B) Quantification of the number of cells showing a polarized distribution of Gag (30 cell conjugates from two independent experiments). (C and D) The ability of primary $CD4^+$ T cells from a GS patient and the corresponding healthy control (C) and Rab27a-silenced or control MDMs co-cultured with autologous $CD4^+$ T cells to form virological synapses (D) was also evaluated by 3D deconvolution fluorescence microscopy and LSCM, respectively. Representative confocal and DIC images are shown. In C, a 3D maximum intensity projection of 10 optical sections acquired at 0.2-µm intervals is shown. (E) 4,800 HIV-infected control or Rab27a-silenced Jurkat cells present in a total of 80,000 cells (Donor cells, left) were added to GHOST cell cultures either allowing direct interaction or separated by a 0.2-µm pore filter (transwell). After 1.5 h of co-culture, cells were removed, and the percentage of GFP-positive GHOST cells was determined by FACS analysis 48 h later. FSC-H, forward scatter height. The boxes contain GFP-positive cells. Histograms show the means ± SD of three experiments performed in triplicates. *, $P < 0.01$; ***, $P < 0.001$. KD, knockdown. Bars, 2 µm.

macrophages, PH-GFP and CD81, did not label any intracellular compartment (Fig. 6, H and I). These changes in $PI(4,5)P_2$ distribution were accompanied by the presence of PM patches containing both $PI(4,5)P_2$ and CD81. Examination of the phase contrast image of the same cell reveals that these patches were located in thicker parts of the PM, thus likely representing areas of stronger fluorescence signal.

Confirming the specificity of the phenotype described in this section, rescue experiments performed in Jurkat cells reverted the decrease in PM levels of $PI(4,5)P_2$ (Fig. 6 J). Altogether, results presented in this section indicate that Rab27a regulates $PI(4,5)P_2$ levels in the PM of $CD4^+$ T cells and in VCCs of MDMs.

Rab27a controls PM levels of PI(4)P and the recruitment of PI4KIIα to the PM

To gain further mechanistic insight, the subcellular distribution of PI(4)P (a precursor in $PI(4,5)P_2$ biosynthesis; Doughman et al., 2003) was analyzed in cells expressing the PI(4)P biosensor GFP-P4M (Hammond et al., 2014). In control Jurkat cells, PI(4)P was detected at the PM as well as in intracellular vesicles that likely represent endosomes and/or the Golgi complex (Fig. 7 A). Interestingly, in Rab27a-silenced cells, there was a selective loss of PM PI(4)P (Fig. 7, A–C). Because of its previously described association with late endosomes (Salazar et al., 2005; Minogue et al., 2006) and its role in PM PI(4)P production (Wei et al., 2002; Balla and Balla, 2006; Pizarro-Cerdá et al., 2007;

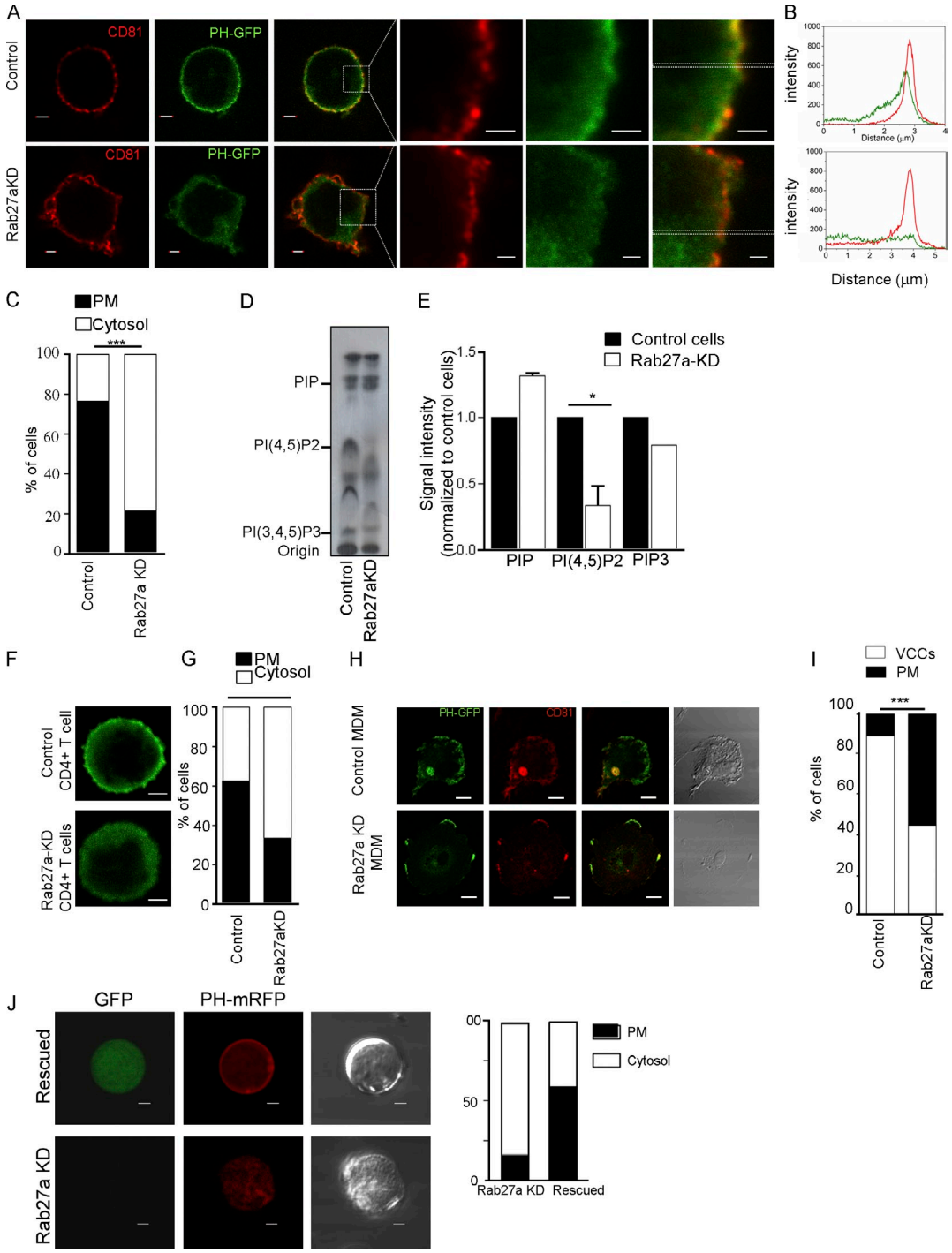

Figure 6. **Silencing of Rab27a reduces PI(4,5)P_2 levels in the PM of CD4$^+$ T cells and in VCCs of macrophages.** (A) LSCM visualization of PH-GFP in control and Rab27a-silenced Jurkat cells. Cell surface CD81 was labeled in nonpermeabilized cells and used as a reference of PM localization. Boxes indicate areas magnified on the right. (B) Representative single-cell intensity profile plots of the fluorescence of PH-GFP and CD81 at the PM quantified in a confocal slice along a line located on a representative segment of the cell (indicated with a scattered white line in the zoom shown in A). (C) Quantification of the localization of the PH-GFP signal predominantly at the PM or the cytosol in control and Rab27a-silenced cells was performed by blinded observers on a per-cell basis, in 200 cells of each condition. Data are expressed as percentages of cells in each category. (D) Incorporation of ^{32}P in phosphoinositides was evaluated by TLC separation of lipid extracts from cells pulsed with [^{32}P]orthophosphate. Shown is a representative autoradiograph. Positions of (phosphatidylinositol monophosphates [PIP]) and PI(4,5)P_2 standards are indicated. (E) Quantification of the relative amounts of different phosphoinositides (n = 3). Error bars show SDs. (F) LSCM images of PH-GFP distribution in Rab27a-silenced primary CD4$^+$ T cells isolated from blood. (G) Quantification of the localization of the PH-GFP signal predominantly at the PM or the cytosol of control and Rab27a-silenced CD4$^+$ T cells. 200 cells were evaluated for each condition. (H) Representative LSCM images showing PH-GFP and CD81 distribution in control and Rab27a-silenced MDMs. (I) Quantification of the percentages of cells containing PH-GFP/CD81 double-positive structures in VCCs or at the peripheral PM. 90 cells were evaluated for each condition. (J and K) Restoring Rab27a expression in Jurkat cells expressing the 3′UTR Rab27a shRNA rescues PI(4,5)P_2 levels at the PM. (J) Representative images of PH-mRFP distribution in Rab27a-silenced cells (using the 3′UTR shRNA) that were transduced (green cell) or not transduced with the Rab27a-encoding lentivirus. (K) Quantifications were performed by blinded observers on a per-cell basis, in ≥30 cells of each condition. Data are expressed as percentages of cells in each category. *, $P < 0.01$; ***, $P < 0.001$. KD, knockdown. Bars: (A [left], F, H, and J) 2 μm; (A, right) 1 μm.

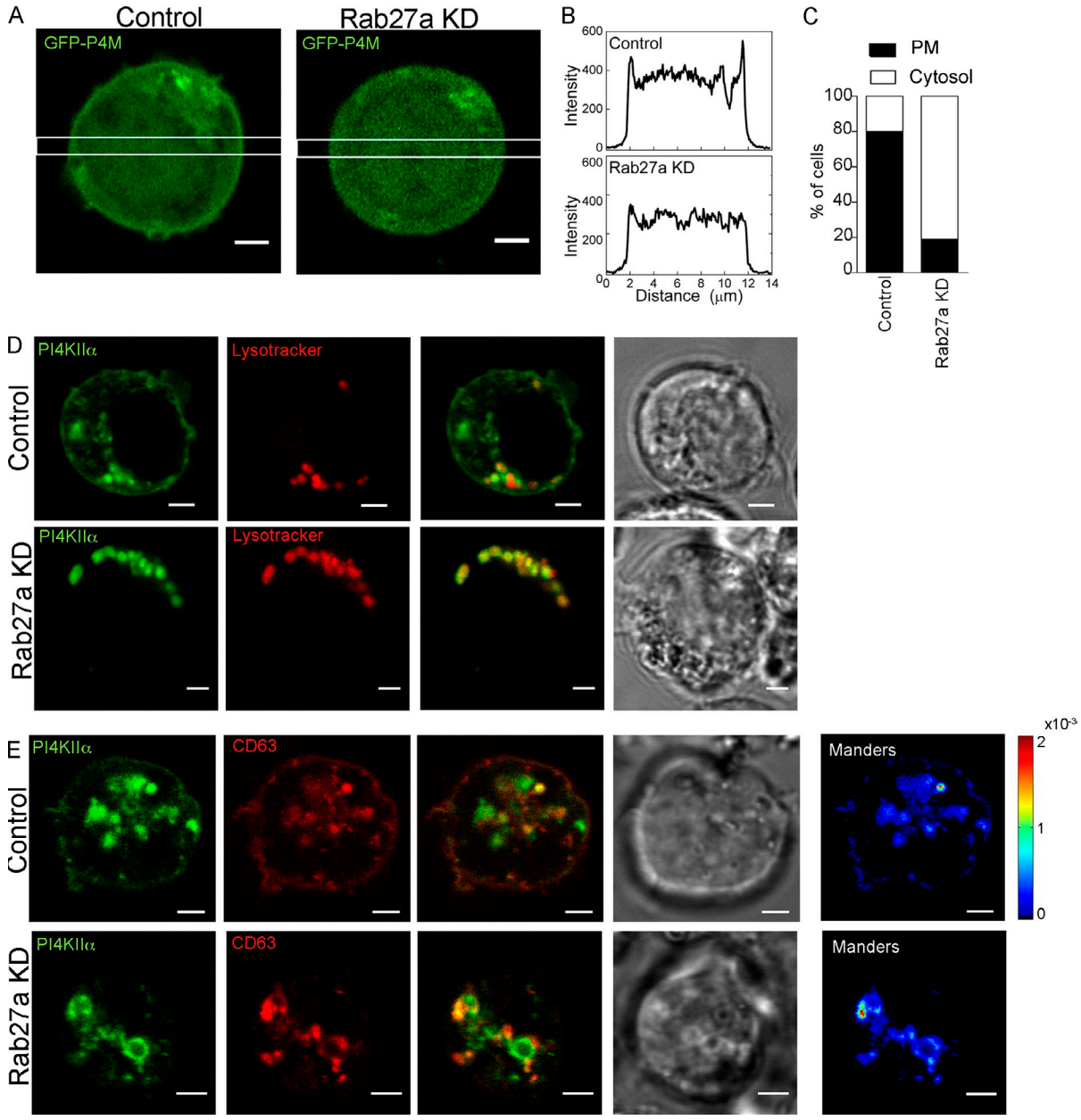

Figure 7. **Rab27a controls PM levels of PI(4)P and the CD63-mediated recruitment of PI4KIIα to the PM.** (A) LSCM images of live control and Rab27a-silenced Jurkat cells transiently transfected with GFP-P4M-SidM plasmid and observed 24 h later. (B) Representative single-cell intensity profile plots of the mean fluorescence intensity of GFP-P4M-SidM quantified in the selected regions indicated with a white rectangle shown in A. (C) Quantification of the localization of the GFP-P4M-SidM signal predominantly at the PM or the cytosol in control and Rab27a-silenced cells was performed by blinded observers on a per-cell basis, in 200 cells of each condition. (D) LSCM of live control and Rab27a-silenced Jurkat cells transiently transfected with PI4KIIα-GFP plasmid and labeled with LysoTracker red. (E) LSCM of live control and Rab27a-silenced Jurkat cells transiently transfected with PI4KIIα-GFP and mCherry-CD63 plasmids. Manders correlation coefficient map is shown. Pseudocolored scale represents the contribution of each pixel to Manders colocalization coefficient (overlap coefficients for control and Rab27a-silenced cells: 0.74 ± 0.01 and 0.75 ± 0.02, respectively). Transmitted light images are shown on the right images of D and E. KD, knockdown. Bars, 2 µm.

Pan et al., 2008), we hypothesized that Rab27a was required for the recruitment of PI4KIIα to the PM from endosomes. Indeed, in control cells, PI4KIIα was located at the PM as well as in intracellular acidic (LysoTracker$^+$) compartments (Fig. 7 D). In agreement with previous studies (Berditchevski et al., 1997; Yauch and Hemler, 2000), we observed that PI4KIIα biochemically interacted with CD63 (Fig. S5 A). Accordingly, we observed that both at the PM and in endosomes, PI4KIIα colocalized with CD63 (Fig. 7 E). Live-cell visualization of cells expressing GFP-PI4KIIa and mCherry CD63 evidenced that some CD63/PI4KIIα double-positive compartments presented rapid and long-range movements. In particular, we observed vesicles that approached the PM where they seemed to dock for several seconds (Video 1 and Fig. S5 B). Further suggesting a role of Rab27a in the trafficking of PI4KIIα, we observed that both molecules colocalized in intracellular structures (Fig. S5 C).

Paralleling the alterations in CD63 distribution (Fig. 2), in Rab27a-silenced cells, PI4KIIα accumulated in enlarged

acidic structures, whereas its localization at the PM was markedly reduced (Fig. 7 D). The biochemical interaction between CD63 and PI4KIIα was not altered in Rab27a-silenced cells (Fig. S5 A). Indeed, CD63 and PI4KIIα colocalized in enlarged endosomes, and both molecules were barely detected at the PM (Fig. 7 E). Live-cell visualization of CD63/PI4KIIα dynamics in Rab27a-silenced cells showed that the enlarged PI4KIIα-positive endosomes did not undergo long-range movements toward the cell periphery (Video 2 and Fig. S5 B). Altogether, these observations suggest that Rab27a controls the intracellular trafficking of CD63/PI4KIIα double-positive endosomes and the delivery of PI4KIIα to the PM, thus promoting PI(4)P and PI(4,5)P_2 production at this location.

Slp2a is a Rab27a effector required for the delivery of PI4KIIα to the PM and for HIV-1 replication in CD4+ T cells

We next sought to identify the Rab27a effector proteins that are required for HIV-1 production. A total of seven out of the nine Rab27a effector proteins analyzed were found to be expressed in Jurkat cells (Table S1). The expression of each individual effector was silenced, and cells were then infected with HIV-1. Silencing of the genes EXPH5, SYTL2, and SYTL3, encoding the proteins Slac2b, Slp2a, and Slp3, respectively, reduced the extracellular release of p24 by ≥50% with ≥2 of the shRNA sequences that were used to target each gene (Fig. 8 A). The inhibition of HIV-1 replication was consistent with a reduction in the expression levels of EXPH5 and SYTL3, as determined by quantitative RT-PCR (qPCR; Fig. 8 B) and of Slp2a, as determined by immunoblotting (Fig. 8 C). We then selected one shRNA targeting each gene to analyze the kinetics of HIV-1 replication in large-scale cultures, using control and Rab27a-silenced cells for comparative purposes. The inhibition of HIV-1 replication in these experiments further confirmed the involvement of Slp2a, Slac2b, and Slp3 in HIV-1 replication (Fig. 8 D). Furthermore, LSCM visualization showed that silencing the expression of Slp2a, Slp3, and Slac2-b led to a diffuse intracellular Gag staining pattern accompanied by a dramatic reduction in the association of $Pr55^{Gag}$ with the PM (Fig. 8 E).

We then decided to further analyze the mechanistic basis of the inhibition of HIV-1 replication by Slp2a, an effector that has been previously shown to play an important role in vesicle docking, in particular in $CD8^+$ T lymphocytes (Ménasché et al., 2008). First, we observed that Rab27a and the hematopoietic isoform of Slp2a, Slp2a-hem, colocalized on the same intracellular vesicular structures (Fig. 8 F). We next analyzed the subcellular distribution of CD63, PI4KIIα, PI(4)P, and PI(4,5)P_2 in Slp2a-silenced cells. An intracellular accumulation of CD63-positive compartments concurrent with a decrease in PM levels of CD63 was observed (Fig. 8 G). Furthermore, we observed that PI4KIIα levels at the PM were dramatically reduced and that the enzyme accumulated at intracellular structures (Fig. 8 H). Consistent with a reduction in PM levels of PI4KIIα, PM levels of PI(4)P (Fig. 8 I) and PI(4,5)P2 (Fig. 8 J) were reduced.

Analysis of CD63 and PI4KIIα interaction showed that both molecules still interacted in Slp2a-silenced cells (Figs. 8 K and S5 A). Interestingly, live-cell visualization showed that, as in the case of Rab27a-silenced cells, both molecules were present in enlarged endosomes that exhibited limited movement. Moreover, the presence of both molecules at the PM was markedly reduced (Video 3 and Fig. S5 B). Altogether, these observations show that Rab27a and Slp2a function together in the trafficking of PI4KIIα/CD63-positive endosomes toward the PM, thus contributing to the generation of PI(4)P and a pool of PI(4,5)P_2 that is required for HIV-1 assembly.

Discussion

In this study, we show that in $CD4^+$ T cells, Rab27a controls the intracellular trafficking of PI4KIIα-positive late endosomes and the recruitment of this enzyme to the PM. Therefore, Rab27a promotes the production of PM PI(4)P and a pool of PI(4,5)P_2 required for $Pr55^{Gag}$ membrane association and HIV-1 assembly. Moreover, we show that Rab27a regulates PI(4,5)P_2 production in the VCCs of macrophages. These results provide new information about the function of Rab27a and reveal that a common pathway regulated by Rab27a is required for HIV-1 production in the two principal target cells of HIV-1 infection.

The main precursor for PI(4,5)P_2 synthesis at the PM is PI(4)P, a product of the activity of a PI4-kinase acting on phosphatidylinositol (Doughman et al., 2003). Although in some cell types, PI(4)P production at the PM is performed by PI4KIIIα (Nakatsu et al., 2012), PI4KIIα has also been shown to control cellular levels of PI(4,5)P_2 (Pan et al., 2008; Chu et al., 2010; Kang et al., 2013). Indeed, despite the fact that in several cell types PI4KIIα localizes primarily to the trans-Golgi network and endosomes (Wang et al., 2003; Salazar et al., 2005; Balla and Balla, 2006; Minogue et al., 2006), a portion of PI4KIIα can be recruited to the PM (Wei et al., 2002; Pizarro-Cerdá et al., 2007). In line with these observations, our results not only show that PI4KIIα is found in late endosomes but also that, by regulating the trafficking of these endosomes, Rab27a allows the recruitment of the enzyme to the PM of $CD4^+$ T cells. Consequently, Rab27a induces PI(4,5)P_2 production, thus favoring the recruitment of $Pr55^{Gag}$. After its association with the PM, $Pr55^{Gag}$ functions as a microdomain-organizing factor, inducing the coalescence of preformed PM domains, such as TEMs and lipid rafts (Krementsov et al., 2010; Hogue et al., 2011; Kerviel et al., 2013), creating a novel virus–induced PM domain used as a platform for HIV-1 assembly and budding. Therefore, our results suggest that HIV-1 assembly is functionally coupled to the trafficking and fusion of late endosomes with the PM.

The cytosolic accumulation of $Pr55^{Gag}$ in Rab27a-silenced cells is in agreement with previous studies showing that, in $CD4^+$ T cell lines, depletion of PI(4,5)P_2 by overexpression of phosphoinositide 5-phosphatase IV induces redistribution of $Pr55^{Gag}$ to a predominantly cytosolic localization (Monde et al., 2011). In contrast, depletion of PM PI(4,5)P_2 in HeLa cells induces Gag accumulation in CD63-positive MVEs (Ono et al., 2004). Although the basis for these cell type–dependent differences is not clear, these observations indicate that the role played by endosomes in Gag membrane targeting and HIV-1 assembly is different in $CD4^+$ T cells and MDMs, as compared

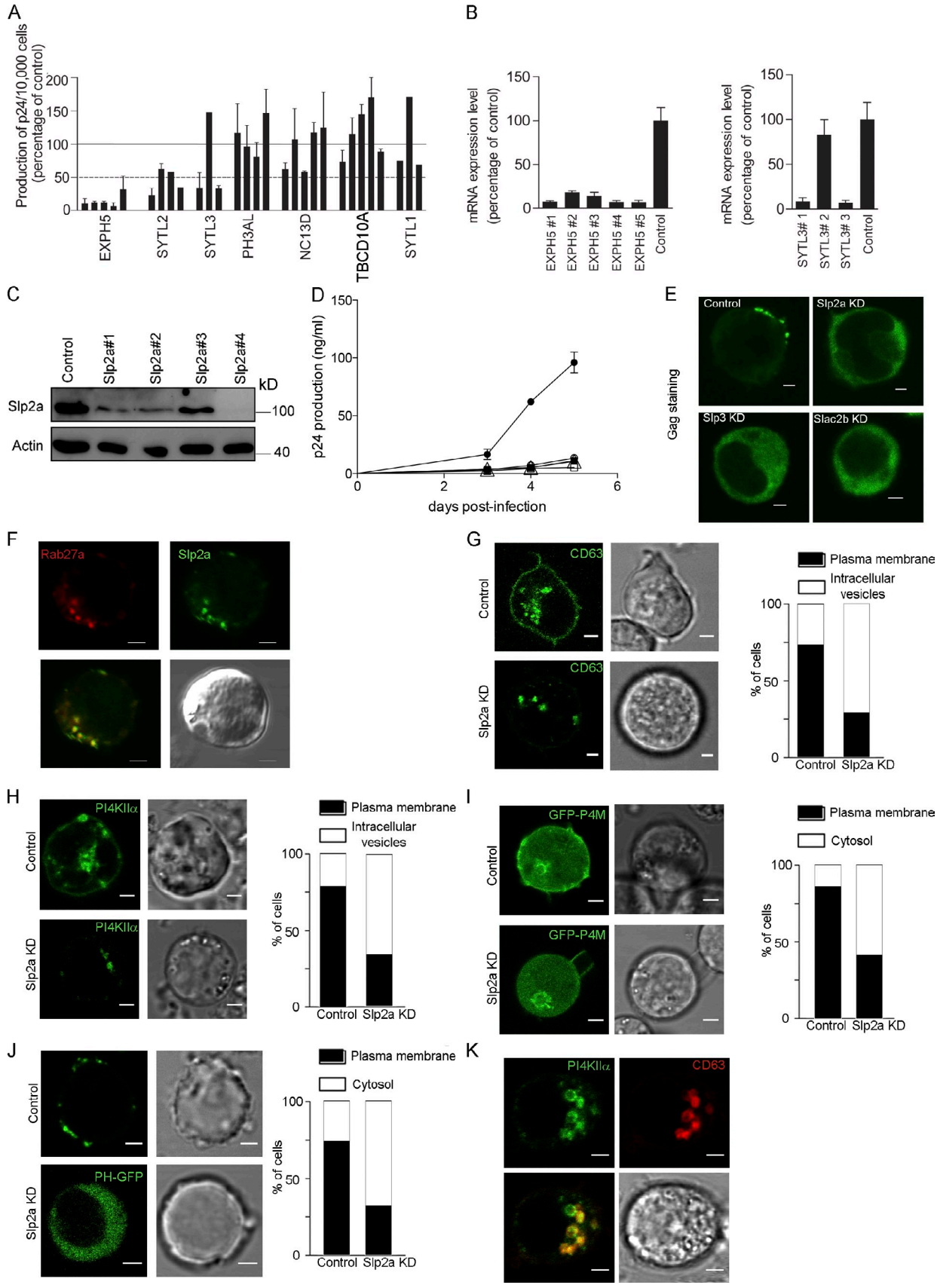

Figure 8. **Slp2a is a Rab27a effector required for PM delivery of PI4KIIα and HIV-1 assembly.** (A) p24 production by Jurkat cells transduced with different shRNAs targeting Rab27 effector genes and subsequently infected with a VSV-G–pseudotyped HIV-1 strain was evaluated at day 4 p.i. Data are the means ± SD of three independent experiments. Solid lines and dashed lines indicate 100% and 50%, respectively, of p24 production by control cells.

with HeLa cells. Along these lines, by using viral variants harboring mutations that block Gag-PI(4,5)P_2 binding and target Gag to MVEs, it has been suggested that CD4$^+$ T cells and MDMs rely more heavily on an endosome-to-PM trafficking pathway, as compared with HeLa cells (Joshi et al., 2009). In agreement with these results, we observed that whereas inhibition of Rab27a expression in HeLa cells induces a profound decrease in the docking of MVEs to the PM (Ostrowski et al., 2010), the reduction in PI(4,5)P_2 levels at the PM and, consequently, HIV-1 assembly are not perturbed in this model cell line (unpublished data). The existence of different or alternative pathways of PI(4,5)P_2 production and HIV-1 assembly in HeLa versus hematopoietic cells will be addressed in future studies.

Despite the unequivocal presence of tetraspanins at HIV-1 exit sites, their role during HIV-1 assembly remains an open question (Chen et al., 2008; Ruiz-Mateos et al., 2008; Grigorov et al., 2009; Krementsov et al., 2009; Li et al., 2014). The difficulty in defining the role played by tetraspanins during the late stages of HIV-1 replication is probably a result of the fact that compensatory mechanisms are likely to take place between the more than 33 members of the tetraspanin family. Our results show that by promoting the fusion of late endosomes with the PM, Rab27a controls the levels of CD63 (and very likely other endosomal tetraspanins) at this location. The biochemical association between CD63 and PI4KIIα suggests the localized production of PI(4)P at TEMs followed by the subsequent production of PI(4,5)P_2. These findings could thus represent the biochemical basis of the association of Pr55^{Gag} with TEMs.

The different roles played by Rab27 are determined by the interaction with a different set of downstream effectors specialized in different functions. Herein, we found that in Jurkat cells, silencing of three different effectors, Slac2b, Slp2a, and Slp3, reduces Pr55^{Gag} membrane association and HIV-1 replication. These results suggest a nonredundant and cooperative mode of action, in which the three Rab27 effectors work jointly in the Rab27a-controlled pathway. A similar mode of interaction has been observed in neuroendocrine PC12 cells, in which four Rab27 effectors, Slp4-a, Slac2-c, Rabphilin, and Noc2 contribute to the docking of granules to the PM (Desnos et al., 2003; Tsuboi and Fukuda, 2005, 2006). Further analysis of the role played by Slp2a allowed us to conclude that silencing this Rab27a effector phenocopies Rab27a-silenced cells, resulting in a reduction in PM levels of CD63, PI4KIIa, PI(4)P, and PI(4,5)P_2. These results, together with previous studies showing that Slp2a is a critical docking factor (Ménasché et al., 2005), suggest that by recruiting Slp2a to CD63$^+$ endosomes, Rab27a promotes the docking of these endosomes to the PM, allowing their fusion and the consequent delivery of PI4KIIa.

In conclusion, this study demonstrates that Rab27a regulates PI(4,5)P_2 levels at the PM of CD4$^+$ T cells and in macrophage VCCs. Thus, Rab27a controls membrane association of Pr55^{Gag} and, consequently, is required for HIV-1 replication.

Materials and methods

Cell lines, plasmids, lentiviral vectors, and HIV-1 viral strains

The human CD4$^+$ T cell line Jurkat clone E6.1, the HIV-1 infection reporter human osteosarcoma cell line GHOST X4/R5, the HIV-1 BaL strain (using CCR5 coreceptor), and the HIV-1 IIIB strain (using CXCR4 coreceptor) were obtained from the AIDS Reagent Program, Division of AIDS, National Institute of Allergy and Infectious Diseases, National Institutes of Health. HEK 293T cells were obtained from ATCC (CRL-11268).

The following plasmids were used: pEGFP-bos-CD63 and mCherry-bos-CD63 encoding full-length CD63 in pEGFP-C1-bos or pmCherry-C1-bos backbone, respectively, under the Bos promoter (provided by G. Griffiths, Cambridge Institute for Medical Research, Cambridge, England, UK; Blott et al., 2001); GFP-P4M-SidM encoding the P4M domain from *Legionella pneumophila* fused to EGFP in the pEGFP-C1 backbone under cytomegalovirus (CMV) promoter (Addgene plasmid 51469; Hammond et al., 2014); pEGFP-C3-Rab27a encoding full-length Rab27a in the pEGFP-C3 backbone under the CMV promoter (Hume et al., 2001); pEGFP-N1-PI4K2A encoding full-length PI4K2A in the pEGFP-N1 backbone under the CMV promoter (provided by T. Balla, Eunice Kennedy Shriver National Institute of Child Health and Human Development, Bethesda, MD; Jović et al., 2012); pEGFP-C1-Slp2a-hem encoding the hematopoietic form of Slp2-a in the pEGFP-C1 backbone under the CMV promotor (provided by G. de Saint Basile, Centre de Référence pour les Déficits Immunitaires Héréditaires, Paris, France; Ménasché et al., 2008); Rab27a-2A-GFP encoding full-length Rab27a fused to a 2A peptide sequence from *Thosea asigna* virus followed by EGFP in pcDNA HIV SIN PZ-CG-FRW-ΔNP (Z-368) under the CMV promoter (provided by M. Zhang and R. Cron, University of Alabama at Birmingham, Birmingham, AL); pBR-NL4.3-IRES-EGFP-Nef$^+$ encoding full-length HIV-1 in the pBR322 backbone under the control of viral long terminal repeat promoter (provided by F. Kirchhoff, Institute of Molecular Virology, Ulm University Medical Center, Ulm, Germany; Schindler et al., 2005); PH-GPF encoding the PH domain of phospholipase C δ1 subunit fused to GFP in pWPT-GFP under the EF1α promoter (provided by R. Galandrini, Istituto Pasteur-Fondazione Cenci-Bolognetti, Fondazione Eleonora Lorillard Spencer Cenci, Sapienza University, Rome, Italy; Micucci et al., 2006).

Lentiviruses were produced as described elsewhere (Moffat et al., 2006). In brief, 2.5 × 10^3 HEK293T were seeded on a flat-bottom 96-well plate. 24 h later, cells were transfected with a mix of 100 ng pCMV-dR8.2 ΔVpr, 100 ng of the target's specific shRNA in the pLKO.1 backbone, and 10 ng pCMV–VSV-G per well, using X-tremeGENE HP DNA transfection reagent (Roche), following the manufacturer's recommendations. 24 h later, medium was replaced, and supernatants containing lentiviral particles were collected at 48 and 72 h after transfection, precleared by centrifugation, aliquoted, and stored at −80°C.

The sequences of the shRNA used are: RAB27A#1, 5′-CCGGCGGATCAGTTAAGTGAAGAAACTCGAGTTTCTTCACTTAACTGATCCGTTTTT-3′; RAB27A#2, 5′-CCGGGCTGCCAATGGGACAAACATACTCGAGTATGTTTGTCCCATTGGCAGCTTTTT-3′; RAB27A targeting the 3′UTR region, 5′-GTACCGGGATCTTCTCTATGATTGATACCTCGAGGTATCAATCATAGAGAAGATCTTTTTTG-3′; MLPH#1, 5′-CCGGCCTTTAGGACAATGTTGTGTACTCGAGTACACAACATTGTCCTAAAGGTTTTTTG-3′; MLPH#2, 5′-CCGGGTCTTCTGAGAGTCAGATCTTCTCGAGAAGATCTGACTCTCAGAAGACTTTTTTG-3′; MLPH#3, 5′-CCGGCTGATCTGTGAGAAACAGCTACTCGAGTAGCTGTTTCTCACAGATCAGTTTTTTG-3′; MLPH#4,

(B) Inhibition of gene expression of EXPH5 and SYTL3 was determined by qPCR (n = 2). (C) Inhibition of Slp2a expression was determined by immunoblotting. (D) Kinetics of HIV-1 (strain IIIB; inoculum: 100 ng/ml) production by Jurkat cells stably transduced with control shRNA (closed circles), SYTL2 shRNA 1 (open squares), EXPH5 shRNA1 (open circles), and SYTL3 shRNA 1 (open triangles). Rab27a-silenced cells were included for comparative purposes (closed squares). One representative experiment of two performed in triplicates is shown. (E) Intracellular distribution of Gag in control or Slac2-b–, Slp2a-, and Slp3-silenced cells was analyzed by LSCM at day 7 p.i. (F) LSCM visualization of cells transiently transfected with dsRed-Rab27a and Slp2a-GFP. (G–J) LSCM of live control and Rab27a-silenced cells stably expressing CD63-GFP (G), PI4KIIa-GFP (H), GFP-P4M (I), and PH-GFP (J). Representative confocal images (left) and transmitted light images (right) are shown. Quantifications were performed by blinded observers on a per-cell basis, in ≥50 cells of each condition. (K) LSCM of live Slp2a-silenced Jurkat cells transiently transfected with PI4KIIα-GFP and mCherry-CD63 plasmids. Error bars show SDs. KD, knockdown. Bars, 2 µm.

5′-CCGGGATCGGAAATCAGTGTACCGACTCGAGTCGGTACACTG-ATTTCCGATCTTTTTTG-3′; MLPH#5, 5′-CCGGCAGTACAACAGGACC-ACAGATCTCGAGATCTGTGGTCCTGTTGTACTGTTTTTTG-3′; EXPH5#1, 5′-CCGGCCGCTTAATATCTATGAGGATCTCGAGATCCTCATAGATAT-TAAGCGGTTTTTTG-3′; EXPH5#2, 5′-CCGGCCGCACACAGATAAAT-CCAATCTCGAGATTGGATTTATCTGTGTGCGGTTTTTTG-3′; EXPH5#3, 5′-CCGGCCCAAACTAGAAGAAGTTCTTCTCGAGAAGAACTTCTTCT-AGTTTGGGTTTTTTG-3′; EXPH5#4, 5′-CCGGCCTCTATCGTTCAAA-GAGTTTCTCGAGAAACTCTTTGAACGATAGAGGTTTTTTG-3′; EXPH5#5, 5′-CCGGGCCAAGAGAAAGGACATTCTTCTCGAGAAGAATGTCCTTT-CTCTTGGCTTTTTTG-3′; SYTL1#1, 5′-CCGGCCTGGACACTTACGTAC-AATGCTCGAGCATTGTACGTAAGTGTCCAGGTTTTTG-3′; SYTL1#2, 5′-CCGGGGCGGTGAAGAAACGGAATCTCTCGAGAGATTCCGTTTCTT-CACCGCCTTTTTG-3′; SYTL1#3, 5′-CCGGTGACCTTGTCCGAGCGTC-TATCTCGAGATAGACGCTCGGACAAGGTCATTTTTG-3′; SYTL1#4, 5′-CCGGTCAACGAGACTCTCCGGTACTCTCGAGAGTACCGGAGAG-TCTCGTTGATTTTTG-3′; SYTL1#5, 5′-CCGGACATCTTTCTGGGCGAA-GTTGCTCGAGCAACTTCGCCCAGAAAGATGTTTTTTG-3′; SYTL2#1, 5′-CCGGTAACGAAATACTGCGGTATAACTCGAGTTATACCGCAG-TATTTCGTTATTTTTG-3′; SYTL2#2, 5′-CCGGCTTAGCAGCAGCGGATG-TAAACTCGAGTTTACATCCGCTGCTGCTAAGTTTTTG-3′; SYTL2#3, 5′-CCGGATTTGGCATCGGGATACATTTCTCGAGAAATGTATCCCGAT-GCCAAATTTTTTG-3′; SYTL2#4, 5′-CCGGGTCGCAGAAAGATACTC-AAAGCTCGAGCTTTGAGTATCTTTCTGCGACTTTTTG-3′; SYTL2#5, 5′-CCGGTCAACCACACTATGGTGTATGCTCGAGCATACACCATAGTGT-GGTTGATTTTTG-3′; SYTL3#1, 5′-CCGGGAGAAATACGAAGACAGC-GTTCTCGAGAACGCTGTCTTCGTATTTCTCTTTTTTG-3′; SYTL3#2, 5′-CCGGCGGAGAGTGTTTCTTGGAGAACTCGAGTTCTCCAAGAAA-CACTCTCCGTTTTTTG-3′; SYTL3#4, 5′-CCGGGCACCTTGAACTCATTT-GTTACTCGAGTAACAAATGAGTTCAAGGTGCTTTTTTG-3′; SYTL3#5, 5′-CCGGCAAATGCTCTACTAACCCTATCTCGAGATAGGGTTAGTA-GAGCATTTGTTTTTTG-3′; MYRIP#1, 5′-CCGGGCCAAATAAGTGCA-AAGATTTCTCGAGAAATCTTTGCACTTATTTGGCTTTTTG-3′; MYRIP#2, 5′-CCGGCCCAGGTACAAACCATAGATACTCGAGTATCTATGGTTTGTA-CCTGGGTTTTTG-3′; MYRIP#3, 5′-CCGGGCTTCGACATTCTAGGAGG-AACTCGAGTTCCTCCTAGAATGTCGAAGCTTTTTG-3′; MYRIP#4, 5′-CCGGGCTGTACGAGTTAGCAATGAACTCGAGTTCATTGCTAAC-TCGTACAGCTTTTTG-3′; MYRIP#5, 5′-CCGGCCTGCAGAAGATTATAC-GAAACTCGAGTTTCGTATAATCTTCTGCAGGTTTTTG-3′; RPH3AL#1, 5′-CCGGGGCTATCTCCGTTGCTATATTCTCGAGAATATAGCAACGGA-GATAGCCTTTTTG-3′; RPH3AL#2, 5′-CCGGAGGGACCGGAAAGGC-GACAAACTCGAGTTTGTCGCCTTTCCGGTCCCTTTTTTG-3′; RPH3AL#4, 5′-CCGGTAGAGGACAGACTCCCATCCACTCGAGTGGATGGGAGT-CTGTCCTCTATTTTTG-3′; RPH3AL#5, 5′-CCGGCAGGAAGAAAGTCTG-CACCAACTCGAGTTGGTGCAGACTTTCTTCCTGTTTTTG-3′; RPH3AL#6, 5′-CCGGGCAGTGAGCAAAGAGAGGTCTCTCGAGAGACCTCTCTTT-GCTCACTGCTTTTTG-3′; SYTL4#1, 5′-CCGGCCTCACTACAACCATA-CATTTCTCGAGAAATGTATGGTTGTAGTGAGGTTTTTG-3′; SYTL4#2, 5′-CCGGCGGGACACTGTTAATCCACTACTCGAGTAGTGGATTAACAGT-GTCCCGTTTTTG-3′; SYTL4#3, 5′-CCGGCCTCCCTTTACATGGAA-AGATCTCGAGATCTTTCCATGTAAAGGGAGGTTTTTG-3′; SYTL4#4, 5′-CCGGCGCCAAGGAAATAGAGTTGAACTCGAGTTCAACTCTATTTC-CTTGGCGTTTTTG-3′; SYTL4#5, 5′-CCGGGAGTACACTAAATCTGT-GATACTCGAGTATCACAGATTTAGTGTACTCTTTTTG-3′; UNC13D#1, 5′-CCGGGCTTTGCTACATGAACACCAACTCGAGTTGGTGTTCATGTA-GCAAAGCTTTTTTG-3′; UNC13D#2, 5′-CCGGGAGACCTTCATCCTGGAG-TTTCTCGAGAAACTCCAGGATGAAGGTCTCTTTTTTG-3′; UNC13D#3, 5′-CCGGCTTCATGATTACCGTCAAGTTCTCGAGAACTTGACGGTAAT-CATGAAGTTTTTTG-3′; UNC13D#4, 5′-CCGGGATCTTCCACAATACCCTC-AACTCGAGTTGAGGGTATTGTGGAAGATCTTTTTTG-3′; UNC13D#5, 5′-CCGGGATGTGCAAGATGAAGGCCTTCTCGAGAAGGCCTTCATCTTG-CACATCTTTTTTG-3′; TBC1D10A#1, 5′-CCGGGAGTGAGGACACCTACT-TGTACTCGAGTACAAGTAGGTGTCCTCACTCTTTTTTG-3′; TBC1D10A#2, 5′-CCGGCAAGGTGAAGTTACAGCAGAACTCGAGTTCTGCTGTAACTT-CACCTTGTTTTTTG-3′; TBC1D10A#3, 5′-CCGGCCATATAACTACACGG-TTCATCTCGAGATGAACCGTGTAGTTATATGGTTTTTTG-3′; TBC1D10A#4, 5′-CCGGGTTCCCATTCCATGAGATGTTCTCGAGAACATCTCATGGAAT-GGGAACTTTTTTG-3′; and TBC1D10A#5, 5′-CCGGCGCTCCTCTATAT-GACAGAATCTCGAGATTCTGTCATATAGAGGAGCGTTTTTTG-3′.

Antibodies

The following antibodies were used: phycoerythrin (PE)-labeled mouse anti–human CD81 (BD); PE-labeled mouse anti–human CD63 (Invitrogen); rabbit anti–human Rab27a and rabbit anti–human β-actin (Synaptic Systems); PE-labeled mouse anti–humanCD317/Tetherin (eBioscience); FITC-labeled mouse anti–HIV-1 p24 (KC57-FITC; Beckman Coulter); rabbit anti–HIV-1 gp41 (Fitzgerald); Alexa Fluor 594–labeled donkey anti–mouse, Alexa Fluor 488–labeled donkey anti–mouse, biotin-labeled donkey anti–human, and Alexa Fluor 594–labeled donkey anti–rabbit (Jackson ImmunoResearch Laboratories, Inc.); rabbit anti–human Slp2-a (provided by M. Fukuda, Tohoku University, Katahira, Miyagi Prefecture, Japan) was obtained by immunizing rabbits with GST-Slp2-a-SHD followed by affinity purification by exposure to antigen-bound Affi-Gel 10 beads (Imai et al.,2004); rabbit anti–rat PI4KIIα (full length; Guo et al., 2003) was provided by P. De Camilli (Yale University, New Haven, CT); and recombinant human anti–HIV-1 gp120 monoclonal antibody (2G12, produced in CHO cells and subsequently purified by protein A affinity chromatography) from H. Katinger (Buchacher et al., 1994; Trkola et al., 1996) and mouse anti–HIV-1 p24 monoclonal antibody (clone 183-H12-5C) from B. Chesebro (Chesebro et al., 1992) were obtained through the National Institutes of Health AIDS Reagent Program, Division of AIDS, National Institute of Allergy and Infectious Diseases, National Institutes of Health.

Patient with GS

The pediatric patient with GS type 2 carries a homozygous RAB27A exon 3 and 4 deletion leading to a frameshift and a premature stop codon. PBMCs were obtained from the patient and the corresponding age-matched controls, who had provided written informed consent in accordance with procedures at Institut National de la Santé et de la Recherche Médicale (Paris, France).

Preparation of viral stocks

The HIV-1 BaL isolate was propagated onto primary macrophages and collected from the culture supernatants. The HIV-1 IIIB isolate was obtained from H9/HTLV-IIIB supernatants (Popovic et al., 1984). The viruses were concentrated by ultracentrifugation at 28,000 rpm for 90 min at 4°C (L7-65 ultracentrifuge; Beckman Coulter), and the virus pellet was suspended in RPMI 1640 medium. The levels of p24 antigen were determined by ELISA (InnoGenetics), and virus input into assays was a function of p24 antigen concentration.

Degranulation assay and CD63 cell surface translocation

For degranulation assays, 2×10^5 control or Rab27a-silenced primary $CD4^+$ T cells were cultured at 37°C in 200 µl complete RPMI containing 10 µM monensin and 5 µg/ml FITC-conjugated anti-CD63 or isotype control. When indicated, cells were stimulated for 20 min with 25 ng/ml PMA (Sigma-Aldrich) and 1 µg/ml ionomycin (Sigma-Aldrich). Cells were washed and analyzed by FACS.

HIV-1 infection

Macrophages (5×10^4/0.1 ml) were infected with HIV-1 BaL strain (50 ng/ml) for 1.5 h at 37°C. Cells were subsequently washed and incubated for different periods. Jurkat cells, PBMCs, and purified $CD4^+$ T lymphocytes (3×10^4/0.1 ml) were infected by the addition of either HIV-1 IIIB strain (50 ng p24/ml; low MOI) or spinoculated with VSV-G–pseudotyped NL4-3-IRES-EGFP (50 ng p24/ml [low MOI] or 200 ng p24/ml [high MOI]) in the presence of 8 µg/ml of polybrene.

In the screening for Rab27a effector proteins, the number of puromycin-resistant Jurkat cells transduced with the different shRNAs was measured using CellTiter 96 AQueous Non-Radioactive Cell Proliferation Assay (Promega). An equal number of cells were then infected with VSV-G–pseudotyped NL4-3-IRES-EGFP (20 ng p24/ml) to ensure a uniform MOI in all conditions.

Quantification of HIV-1 production

HIV-1 p24 released into the cell culture supernatants was quantified using the Innotest HIV-1 Ag mAb Screening 3 kit (InnoGenetics). The number of living cells present in each well was evaluated using CellTiter 96 AQueous Non-Radioactive Cell Proliferation Assay.

Infectivity assay

For infectivity assays, control and Rab27a-silenced cells were infected with HIV-1 strain IIIb. At day 10 after infection, cell culture supernatants were collected, and their content of p24 was determined by ELISA to allow the normalization for equal amounts of p24. The volume of supernatant equivalent to 10 ng p24 was incubated with 20,000 GHOST cells for 48 h, and the percentage of GFP-positive GHOST cells was determined by FACS analysis.

Lentiviral transduction, gene silencing, and transfection of Jurkat cells

A total of 30,000 Jurkat cells were transduced with lentiviral vectors by spinoculation (2,200 rpm at 90 min for 37°C) in the presence of 8 µg/ml of polybrene. After 48 h, transduced cells were selected by the addition of 3 µg/ml puromycin. Transfection of Jurkat cells was performed using X-tremeGENE HP DNA (Roche) following the manufacturer's instruction.

Primary cells transduction and gene silencing

To silence gene expression in macrophages, monocytes were isolated from buffy coats of healthy anonymous donors from the Blood Center of the Mendez Hospital in Buenos Aires, Argentina. Cells were transduced with the corresponding lentiviral vector together with virus-like particles containing the protein VPx from simian immunodeficiency virus (provided by N. Manel, Institut Curie, Paris, France) in the presence of 30 ng/ml rHuGM-CSF and 2.5 µg/ml polybrene for 5 d following a recently published protocol (Satoh and Manel, 2013). Transduced cells were selected by the addition of 30 µg/ml puromycin. To silence gene expression in primary T lymphocytes, either PBMCs or isolated $CD4^+$ T lymphocytes (purified by using a $CD4^+$ T Cell Isolation kit [Miltenyi Biotec]) were seeded at 2×10^6 cells/ml and stimulated with either 1 µg/ml phyto-HA or with anti-CD3/CD28 beads for 3 d in culture medium supplemented with 10 U/ml IL-2. Subsequently, cells were spinoculated as described in the previous section. After spinoculation, 5 ng/ml rIL-2 was added and refreshed every 3 d.

HIV-1 attachment and entry

For HIV attachment and entry measurements, 50,000 Jurkat cells were infected with HIV-1 strain IIIb (50 ng/ml p24) for 1.5 h at 4°C (attachment) or 37°C (attachment + entry). Cells were then extensively washed (five times) to remove unbound viral input and lysed with radioimmunoprecipitation assay buffer. Total cell protein was calculated using bicinchoninic acid, and all samples were normalized for protein content before quantification of cell-associated p24 by ELISA. Viral attachment (4°C) corresponds to p24 amount measured in samples kept at 4°C, and viral entry corresponds to the difference between p24 from samples kept at 37°C and the ones at 4°C.

Single cycle viral entry assay

A total of 30,000 Jurkat cells were infected with two doses of HIV-1 strain IIIb (50 and 500 ng/ml) for 6 h at 37°C. Cells were then washed to remove extracellular virions, and 5 µM AZT (zidovudine) was added to the culture medium to prevent secondary replication cycles and maintained throughout the study. Alternatively, cells were treated with AZT before HIV-1 infection to evaluate the efficiency of the drug to inhibit HIV-1 replication. Viral entry was assessed by quantifying the percentage of HIV-1–infected cells at 48 h p.i.

HIV-1 release assay

3×10^4/0.1 ml Jurkat cells were spinoculated with a high MOI of VSV-G–pseudotyped HIV-1. 48 h later, 1 ml cell culture supernatants were collected, ultracentrifuged (100,000 g; 90 min), and resuspended in 20 µl of immunoblot loading buffer. Cells were extensively washed and lysed. 20 µg of cell lysate and the totality of the pelleted supernatant were analyzed by immunoblotting using p24 antibodies and actin as a loading control for the cell lysates.

Rab27a shRNA rescue experiments

To rescue the Rab27a knockdown phenotype, exogenous Rab27a was expressed in Jurkat cells in which endogenous Rab27a expression was silenced by using an shRNA targeting the 3′UTR of the Rab27a gene. Expression of exogenous Rab27a was achieved by transducing the cells with a lentiviral vector encoding human Rab27a fused to a 2A peptide sequence from *T. asigna* virus followed by GFP, thus allowing simultaneous expression of Rab27a and GFP. Cells expressing the exogenous Rab27a were identified by visualizing GFP expression in microscopy experiments. Alternatively, to analyze HIV-1 replication, GFP-expressing cells were FACS sorted and subsequently infected with HIV-1.

Cell lysates and immunoblot

Cells were lysed in precooled radioimmunoprecipitation assay buffer (1% Triton X-100, 0.1% SDS, 50 mM Tris, pH 7.5, 150 mM NaCl, and 0.5% sodium deoxycholate), supplemented with a cocktail of antiproteases (Roche), and cleared from nuclei by centrifugation at 15,000 *g* for 5 min. Equal amounts of protein extracts were separated on 4–12% SDS-PAGE, blotted on Polyvinylidene Fluoride Transfer Membrane (Thermo Fisher Scientific). Blots were revealed using SuperSignal West Pico Chemiluminescent Substrate (Thermo Fisher Scientific). Intensity of the bands was quantified using the software ImageJ (National Institutes of Health).

Cell fractionation

Subcellular fractionation was performed using the Qproteome Cell Compartment kit, according to the manufacturer's instructions (QIAGEN). Alternatively, cell fractions were isolated by differential centrifugation as described previously (Cox and Emili, 2006). In brief, 10^7 Jurkat cells were washed twice in PBS and attached extracellular virus was eliminated by incubating the cells with trypsin for 5 min at 37°C. After washing, cells were resuspended in 250 mM sucrose, 50 mM Tris-HCl, pH 7.4, and 5 mM $MgCl_2$ containing protease inhibitor cocktail (Roche). This suspension was passed 40 times through a 29-guage needle to lyse the cells, centrifuged to eliminate nuclei and cells debris, and then ultracentrifuged for 1 h at 100,000 *g*. The supernatant of this ultracentrifugation represents the cytosolic proteins, and the pellet represents the membrane-bound proteins. This pellet was resuspended in 0.5 ml of 20 mM Tris-HCl, 0.4 M NaCl, 15% glycerol, and 1.5% Triton X-100, incubated for 1-h shaking at 1,400 rpm and 4°C, and centrifuged at 9,000 *g* for 30 min. The supernatant contained the isolated membrane proteins.

Immunoprecipitation of GFP-CD63

For immunoprecipitation of GFP-CD63, 10^7 GFP-CD63–transfected cells were lysed in immunoprecipitation buffer (1% Brij 99, 10 mM Tris/HCl, pH 7.4, 150 mM NaCl, and 5 mM EDTA, with Roche protease inhibitor cocktail) for 1 h at 4°C. Precleared supernatants were then immunoprecipitated with GFP-Traps or uncoated agarose beads (as control for unspecific bound) according to manufacturer's instructions (ChromoTek). Coprecipitation of PI4KIIα was revealed by immunoblotting.

qPCR

RNAs were isolated with TRIzol reagent (Life Technologies), and 200-ng RNAs were reverse transcribed with M-MLV Reverse transcription (Invitrogen). 1/10th cDNA was used for each PCR reaction, performed with SYBR green (Applied Biosystems) on a real-time thermal cycler (PRISM 7500; Applied Biosystems). Cycle thresholds (Ct's) were normalized to the Ct of GAPDH, and fold enrichments were calculated as compared with the values from control shRNA-transduced cells.

Cell-to-cell transmission assay

Jurkat cells (donor cells) were infected with the HIV-1 IIIB strain. At day 10 p.i, the percentage of infected cells was determined by intracellular staining of p24 antigen followed by FACS analysis. To have equal numbers of control and Rab27a-silenced HIV-1–infected Jurkat cells, cells were diluted with noninfected control or Rab27a-silenced cells, respectively, to have a total of 4,800 HIV-1–infected donor cells present in a total of 80,000 cells (6%) for each category. Next, cells were added to wells containing 30,000 adherent GHOST cells (target). Donor and target cells were co-cultured at 37°C for 3 h before Jurkat cells were removed by extensive washes. HIV-1 transmission was evaluated 48 h later by analyzing the percentage of GFP-expressing GHOST cells. Alternatively, donor and target cells were separated by a 0.2-µm-diameter pore to allow viral transmission without cell-to-cell contact.

Flow cytometry

For surface labeling, cells were stained with antibodies diluted in PBS–0.5% BSA on ice. For intracellular staining, cells were fixed and permeabilized using Cytofix/Cytoperm reagents (BD) and stained with antibodies diluted in permeabilization buffer. Cells were acquired on a FACSCanto (BD) and analyzed using FACSDiva software (BD).

Fluorescence microscopy

10^5 cells were seeded on poly-L-lysine–coated glass coverslips for 60 min, fixed in 4% paraformaldehyde, quenched with 0.1 M glycine, permeabilized in PBS–0.2% BSA–0.05% saponin, and incubated with primary antibodies, which were subsequently detected with Alexa Flour 594–labeled donkey anti–mouse, Alexa Fluor 488–labeled donkey anti–mouse, or Alexa Fluor 594–labeled donkey anti–rabbit (Jackson ImmunoResearch Laboratories, Inc.) secondary antibodies, as indicated. The coverslips mounted with Fluoromount-G (SouthernBiotech) were examined under a confocal microscope (FluoView FV1000; Olympus) using a Plan Apochromat 60× 1.42 NA oil immersion objective. Images were analyzed using the FV10-ASW

software (Olympus). In Figs. 3 C, 4 C, 5, and 6 (E, F, and H), levels were adjusted using Photoshop 7 (Adobe) for better visualization according to the guidelines for the presentation of digital data.

Fluorescence images of live or fixed cells shown in Figs. 2, 6 A, 7, 8 (F–I), S5 B, and Videos 1–3 were acquired in a spectral confocal microscope (FluoView FV1000; acquisition software FV10-ASW 2.0), at room temperature, using a 60× U Plan S Apochromat, NA 1.35 oil immersion objective, in RPMI 1640 medium supplemented with 10% FCS and 10 nM Hepes. Images and videos were analyzed using FIJI (National Institutes of Health) and Matlab (The MathWorks, Inc.) software, respectively.

In Figs. 3 A and 5 C, images were acquired at room temperature using a motorized upright wide-field microscope (DMRA2; Leica) equipped for image deconvolution. Acquisition was performed using a 100× objective (Plan Apochromat HCX, 1.4 NA) and a high-sensitive cooled interlined charge-coupled device camera (CoolSNAP HQ; Roper Scientific). Z positioning was accomplished by a piezoelectric motor (Linear Variable Differential Transformers LVDT; Physik Instrument), and a z series of images was taken (an image every 0.2 µm). Images were acquired with MetaMorph software (Molecular Devices).

Image processing

In Figs. 3 A and 5 C, deconvolution was performed automatically using an iterative and measured point spread function–based algorithm method (Gold–Meinel) on batches of image stacks, as a service proposed by the Bioimaging Cell and Tissue Core Facility of the Institut Curie, as described in Sibarita (2005). Image panels were assembled with Photoshop; no digital manipulation was applied except for adjustment of brightness and contrast in Figs. 3 (A and B), 4 C, 5, 6 (F and H), and 8 (E and F) using ImageJ software.

Phospholipid labeling and analysis

2×10^6 Rab27a-silenced or control cells were pulsed with 25 µCi/ml of [^{32}P]orthophosphate during 45 min either in TBS buffer or in RPMI 1640 media. Cells were washed tree times with cold TBS, and phosphoinositide phospholipids were extracted by a single-step acidic extraction (Lloyd et al., 1972). In brief, 1 ml cell suspension was mixed with 3.75 ml chloroform/methanol/HCl (12 N; 40:80:1 vol/vol/vol). After mixing, 1.25 ml chloroform was added for 5–10 s followed by 1.25 ml of water with mixing for 5–10 s. The biphasic mixture was centrifuged at 1,000 rpm for 10 min, and the chloroform layer was transferred to another tube and dried (Vickers et al., 1982).

For TLC separation of phosphoinositide phospholipids, Silica Gel 60 TLC plates (Merck) were treated with a solution of 1% potassium oxalate in methanol/water (2:3) and warmed to 110°C for 30 min before use. TLC plates were developed by using a 1D, two-solvent system consisting of mixtures of chloroform/methanol/acetic acid/water, 25:15:8:2 vol/vol/vol/vol for the first run and 25:15:16:2 vol/vol/vol/vol for the second. After TLC plates were dried, they were exposed to the autoradiography film, incubated during 24–72 h at −70°C, and developed. In parallel, polyphosphoinositide standards obtained from Echelon were run under the same conditions and stained by iodine spraying for visualization. The Rf (relative migration factor) for each standard was calculated and used for the identification of the radioactive phospholipid samples developed by autoradiography according to previous studies (Bussolino et al., 2001).

Statistical analyses

Data were analyzed using Prism (GraphPad Software). Normality of the data was tested using the Kolmogorov–Smirnov test. Based on the normality test, either one-way analysis of variance followed by Tukey's after test or Kruskal–Wallis followed by Dunn's after test were used for multiple comparison analyses. Values are given as means ± SD. For the colocalization analysis, Manders overlap coefficient was calculated as previously described (Manders et al., 1993). Manders colocalization maps were obtained by imaging the contribution R_i of each pixel i of the images to the Manders overlap coefficient, calculated following

$$R_i = \frac{S1i \times S2i}{\sqrt{\sum_k (S1k)^2 \times \sum_k (S2k)^2}},$$

where S1i represents the signal intensity of pixels in channel 1, and S2i represents the signal intensity of pixels in channel 2. This analysis was performed through a Matlab-written previously described algorithm (Villalta et al., 2011).

Online supplemental material

Fig. S1 shows rescue experiments for Rab27a functionality. Fig. S2 shows that Rab27a silencing alters neither HIV-1 entry nor tetherin expression. Fig. S3 shows a defect in CD63 translocation to the cell surface in Rab27a-silenced cells in which granule secretion was induced by PMA-ionomycin stimulation. Fig. S4 shows CD63 and CD81 distribution in Jurkat cells. Fig. S5 shows the biochemical association between PI4KIIα and CD63 in control, Rab27a-silenced cells, and Slp2a-silenced cells. Table S1 shows qPCR analysis of the expression of Rab27 effector proteins in Jurkat cells. Video 1 shows localization and dynamics of mCherry-CD63 and GFP-PI4KIIα in control Jurkat cells. Video 2 show localization and dynamics of mCherry-CD63 and GFP-PI4KIIα in Rab27a-silenced Jurkat cells. Video 3 shows localization and dynamics of mCherry-CD63 and GFP-PI4KIIα in Slp2a-silenced Jurkat cells. Online supplemental material is available at http://www.jcb.org/cgi/content/full/jcb.201409082/DC1.

We thank Dr. Mitsunori Fukuda, Dr. Ricciarda Galandrini, Dr. Tamas Balla, Dr. Pietro De Camilli, Dr. Mingce Zhang, Dr. Randy Cron, Dr. Gillian Griffiths, and Dr. Frank Kirchhoff for the kind gift of the reagents detailed in the Materials and methods.

This work was supported by doctoral fellowships from Universidad de Buenos Aires and CONICET to M. Cabrini and P.P. Gerber, respectively, and grants 2010-1681 and 2012-00353 from Agencia Nacional de Promoción Científica y Tecnológica (Argentina) and the Creative and Novel Ideas in HIV Research Program through a supplement to the University of Alabama at Birmingham Center for AIDS Research funding grant P30 AI027767-24 to M. Ostrowski.

The authors declare no competing financial interests.

Submitted: 17 September 2014
Accepted: 1 April 2015

References

Balasubramaniam, M., and E.O. Freed. 2011. New insights into HIV assembly and trafficking. *Physiology (Bethesda)*. 26:236–251. http://dx.doi.org/10.1152/physiol.00051.2010

Balla, A., and T. Balla. 2006. Phosphatidylinositol 4-kinases: old enzymes with emerging functions. *Trends Cell Biol.* 16:351–361. http://dx.doi.org/10.1016/j.tcb.2006.05.003

Benaroch, P., E. Billard, R. Gaudin, M. Schindler, and M. Jouve. 2010. HIV-1 assembly in macrophages. *Retrovirology.* 7:29. http://dx.doi.org/10.1186/1742-4690-7-29

Bennett, A.E., K. Narayan, D. Shi, L.M. Hartnell, K. Gousset, H. He, B.C. Lowekamp, T.S. Yoo, D. Bliss, E.O. Freed, and S. Subramaniam. 2009. Ion-abrasion scanning electron microscopy reveals surface-connected tubular conduits in HIV-infected macrophages. *PLoS Pathog.* 5:e1000591. http://dx.doi.org/10.1371/journal.ppat.1000591

Berditchevski, F., K.F. Tolias, K. Wong, C.L. Carpenter, and M.E. Hemler. 1997. A novel link between integrins, transmembrane-4 superfamily proteins (CD63 and CD81), and phosphatidylinositol 4-kinase. *J. Biol. Chem.* 272:2595–2598. http://dx.doi.org/10.1074/jbc.272.5.2595

Blott, E.J., G. Bossi, R. Clark, M. Zvelebil, and G.M. Griffiths. 2001. Fas ligand is targeted to secretory lysosomes via a proline-rich domain in its cytoplasmic tail. *J. Cell Sci.* 114:2405–2416.

Booth, A.M., Y. Fang, J.K. Fallon, J.M. Yang, J.E. Hildreth, and S.J. Gould. 2006. Exosomes and HIV Gag bud from endosome-like domains of the T cell plasma membrane. *J. Cell Biol.* 172:923–935. http://dx.doi.org/10.1083/jcb.200508014

Buchacher, A., R. Predl, K. Strutzenberger, W. Steinfellner, A. Trkola, M. Purtscher, G. Gruber, C. Tauer, F. Steindl, A. Jungbauer, et al. 1994. Generation of human monoclonal antibodies against HIV-1 proteins; electrofusion and Epstein-Barr virus transformation for peripheral blood lymphocyte immortalization. *AIDS Res. Hum. Retroviruses.* 10:359–369. http://dx.doi.org/10.1089/aid.1994.10.359

Bussolino, D.F., M.E. Guido, G.A. Gil, G.A. Borioli, M.L. Renner, V.R. Grabois, C.B. Conde, and B.L. Caputto. 2001. c-Fos associates with the endoplasmic reticulum and activates phospholipid metabolism. *FASEB J.* 15:556–558.

Carr, J.M., H. Hocking, P. Li, and C.J. Burrell. 1999. Rapid and efficient cell-to-cell transmission of human immunodeficiency virus infection from monocyte-derived macrophages to peripheral blood lymphocytes. *Virology.* 265:319–329. http://dx.doi.org/10.1006/viro.1999.0047

Checkley, M.A., B.G. Luttge, and E.O. Freed. 2011. HIV-1 envelope glycoprotein biosynthesis, trafficking, and incorporation. *J. Mol. Biol.* 410:582–608. http://dx.doi.org/10.1016/j.jmb.2011.04.042

Chen, H., N. Dziuba, B. Friedrich, J. von Lindern, J.L. Murray, D.R. Rojo, T.W. Hodge, W.A. O'Brien, and M.R. Ferguson. 2008. A critical role for CD63 in HIV replication and infection of macrophages and cell lines. *Virology*. 379:191–196. http://dx.doi.org/10.1016/j.virol.2008.06.029

Chesebro, B., K. Wehrly, J. Nishio, and S. Perryman. 1992. Macrophage-tropic human immunodeficiency virus isolates from different patients exhibit unusual V3 envelope sequence homogeneity in comparison with T-cell-tropic isolates: definition of critical amino acids involved in cell tropism. *J. Virol.* 66:6547–6554.

Chu, K.M., S. Minogue, J.J. Hsuan, and M.G. Waugh. 2010. Differential effects of the phosphatidylinositol 4-kinases, PI4KIIα and PI4KIIIβ, on Akt activation and apoptosis. *Cell Death Dis.* 1:e106. http://dx.doi.org/10.1038/cddis.2010.84

Cox, B., and A. Emili. 2006. Tissue subcellular fractionation and protein extraction for use in mass-spectrometry-based proteomics. *Nat. Protoc.* 1:1872–1878. http://dx.doi.org/10.1038/nprot.2006.273

Deneka, M., A. Pelchen-Matthews, R. Byland, E. Ruiz-Mateos, and M. Marsh. 2007. In macrophages, HIV-1 assembles into an intracellular plasma membrane domain containing the tetraspanins CD81, CD9, and CD53. *J. Cell Biol.* 177:329–341. http://dx.doi.org/10.1083/jcb.200609050

Desnos, C., J.S. Schonn, S. Huet, V.S. Tran, A. El-Amraoui, G. Raposo, I. Fanget, C. Chapuis, G. Ménasché, G. de Saint Basile, et al. 2003. Rab27A and its effector MyRIP link secretory granules to F-actin and control their motion towards release sites. *J. Cell Biol.* 163:559–570. http://dx.doi.org/10.1083/jcb.200302157

Dimitrov, D.S., R.L. Willey, H. Sato, L.J. Chang, R. Blumenthal, and M.A. Martin. 1993. Quantitation of human immunodeficiency virus type 1 infection kinetics. *J. Virol.* 67:2182–2190.

Dong, X., H. Li, A. Derdowski, L. Ding, A. Burnett, X. Chen, T.R. Peters, T.S. Dermody, E. Woodruff, J.J. Wang, and P. Spearman. 2005. AP-3 directs the intracellular trafficking of HIV-1 Gag and plays a key role in particle assembly. *Cell*. 120:663–674. http://dx.doi.org/10.1016/j.cell.2004.12.023

Doughman, R.L., A.J. Firestone, and R.A. Anderson. 2003. Phosphatidylinositol phosphate kinases put PI4,5P(2) in its place. *J. Membr. Biol.* 194:77–89. http://dx.doi.org/10.1007/s00232-003-2027-7

Gould, S.J., A.M. Booth, and J.E. Hildreth. 2003. The Trojan exosome hypothesis. *Proc. Natl. Acad. Sci. USA*. 100:10592–10597. http://dx.doi.org/10.1073/pnas.1831413100

Grigorov, B., V. Attuil-Audenis, F. Perugi, M. Nedelec, S. Watson, C. Pique, J.L. Darlix, H. Conjeaud, and D. Muriaux. 2009. A role for CD81 on the late steps of HIV-1 replication in a chronically infected T cell line. *Retrovirology*. 6:28. http://dx.doi.org/10.1186/1742-4690-6-28

Guo, J., M.R. Wenk, L. Pellegrini, F. Onofri, F. Benfenati, and P. De Camilli. 2003. Phosphatidylinositol 4-kinase type IIalpha is responsible for the phosphatidylinositol 4-kinase activity associated with synaptic vesicles. *Proc. Natl. Acad. Sci. USA*. 100:3995–4000. http://dx.doi.org/10.1073/pnas.0230488100

Hammond, G.R., M.P. Machner, and T. Balla. 2014. A novel probe for phosphatidylinositol 4-phosphate reveals multiple pools beyond the Golgi. *J. Cell Biol.* 205:113–126. http://dx.doi.org/10.1083/jcb.201312072

Hogue, I.B., J.R. Grover, F. Soheilian, K. Nagashima, and A. Ono. 2011. Gag induces the coalescence of clustered lipid rafts and tetraspanin-enriched microdomains at HIV-1 assembly sites on the plasma membrane. *J. Virol.* 85:9749–9766. http://dx.doi.org/10.1128/JVI.00743-11

Hume, A.N., L.M. Collinson, A. Rapak, A.Q. Gomes, C.R. Hopkins, and M.C. Seabra. 2001. Rab27a regulates the peripheral distribution of melanosomes in melanocytes. *J. Cell Biol.* 152:795–808. http://dx.doi.org/10.1083/jcb.152.4.795

Imai, A., S. Yoshie, T. Nashida, H. Shimomura, and M. Fukuda. 2004. The small GTPase Rab27B regulates amylase release from rat parotid acinar cells. *J. Cell Sci.* 117:1945–1953. http://dx.doi.org/10.1242/jcs.01048

Jolly, C., and Q.J. Sattentau. 2007. Human immunodeficiency virus type 1 assembly, budding, and cell-cell spread in T cells take place in tetraspanin-enriched plasma membrane domains. *J. Virol.* 81:7873–7884. http://dx.doi.org/10.1128/JVI.01845-06

Jolly, C., S. Welsch, S. Michor, and Q.J. Sattentau. 2011. The regulated secretory pathway in CD4(+) T cells contributes to human immunodeficiency virus type-1 cell-to-cell spread at the virological synapse. *PLoS Pathog.* 7:e1002226. http://dx.doi.org/10.1371/journal.ppat.1002226

Joshi, A., S.D. Ablan, F. Soheilian, K. Nagashima, and E.O. Freed. 2009. Evidence that productive human immunodeficiency virus type 1 assembly can occur in an intracellular compartment. *J. Virol.* 83:5375–5387. http://dx.doi.org/10.1128/JVI.00109-09

Jouve, M., N. Sol-Foulon, S. Watson, O. Schwartz, and P. Benaroch. 2007. HIV-1 buds and accumulates in "nonacidic" endosomes of macrophages. *Cell Host Microbe*. 2:85–95. http://dx.doi.org/10.1016/j.chom.2007.06.011

Jović, M., M.J. Kean, Z. Szentpetery, G. Polevoy, A.C. Gingras, J.A. Brill, and T. Balla. 2012. Two phosphatidylinositol 4-kinases control lysosomal delivery of the Gaucher disease enzyme, β-glucocerebrosidase. *Mol. Biol. Cell*. 23:1533–1545. http://dx.doi.org/10.1091/mbc.E11-06-0553

Kang, M.S., S.H. Baek, Y.S. Chun, A.Z. Moore, N. Landman, D. Berman, H.O. Yang, M. Morishima-Kawashima, S. Osawa, S. Funamoto, et al. 2013. Modulation of lipid kinase PI4KIIα activity and lipid raft association of presenilin 1 underlies γ-secretase inhibition by ginsenoside (20S)-Rg3. *J. Biol. Chem.* 288:20868–20882. http://dx.doi.org/10.1074/jbc.M112.445734

Kerviel, A., A. Thomas, L. Chaloin, C. Favard, and D. Muriaux. 2013. Virus assembly and plasma membrane domains: which came first? *Virus Res.* 171:332–340. http://dx.doi.org/10.1016/j.virusres.2012.08.014

Krementsov, D.N., J. Weng, M. Lambelé, N.H. Roy, and M. Thali. 2009. Tetraspanins regulate cell-to-cell transmission of HIV-1. *Retrovirology*. 6:64. http://dx.doi.org/10.1186/1742-4690-6-64

Krementsov, D.N., P. Rassam, E. Margeat, N.H. Roy, J. Schneider-Schaulies, P.E. Milhiet, and M. Thali. 2010. HIV-1 assembly differentially alters dynamics and partitioning of tetraspanins and raft components. *Traffic*. 11:1401–1414. http://dx.doi.org/10.1111/j.1600-0854.2010.01111.x

Li, G., M.A. Endsley, A. Somasunderam, S.L. Gbota, M.I. Mbaka, J.L. Murray, and M.R. Ferguson. 2014. The dual role of tetraspanin CD63 in HIV-1 replication. *Virol. J.* 11:23. http://dx.doi.org/10.1186/1743-422X-11-23

Lloyd, J.V., E.E. Nishizawa, J. Haldar, and J.F. Mustard. 1972. Changes in 32 p-labelling of platelet phospholipids in response to ADP. *Br. J. Haematol.* 23:571–585. http://dx.doi.org/10.1111/j.1365-2141.1972.tb07092.x

Manders, E.M.M., F.J. Verbeek, and J.A. Aten. 1993. Measurement of colocalization of objects in dual-color confocal images. *J. Microsc.* 169:375–382. http://dx.doi.org/10.1111/j.1365-2818.1993.tb03313.x

Ménasché, G., J. Feldmann, A. Fischer, and G. de Saint Basile. 2005. Primary hemophagocytic syndromes point to a direct link between lymphocyte cytotoxicity and homeostasis. *Immunol. Rev.* 203:165–179. http://dx.doi.org/10.1111/j.0105-2896.2005.00224.x

Ménasché, G., M.M. Ménager, J.M. Lefebvre, E. Deutsch, R. Athman, N. Lambert, N. Mahlaoui, M. Court, J. Garin, A. Fischer, and G. de Saint Basile. 2008. A newly identified isoform of Slp2a associates with Rab27a in cytotoxic T cells and participates to cytotoxic granule secretion. *Blood*. 112:5052–5062. http://dx.doi.org/10.1182/blood-2008-02-141069

Micucci, F., A. Zingoni, M. Piccoli, L. Frati, A. Santoni, and R. Galandrini. 2006. High-efficient lentiviral vector-mediated gene transfer into primary human NK cells. *Exp. Hematol.* 34:1344–1352. http://dx.doi.org/10.1016/j.exphem.2006.06.001

Minogue, S., M.G. Waugh, M.A. De Matteis, D.J. Stephens, F. Berditchevski, and J.J. Hsuan. 2006. Phosphatidylinositol 4-kinase is required for endosomal trafficking and degradation of the EGF receptor. *J. Cell Sci.* 119:571–581. http://dx.doi.org/10.1242/jcs.02752

Mlcochova, P., A. Pelchen-Matthews, and M. Marsh. 2013. Organization and regulation of intracellular plasma membrane-connected HIV-1 assembly compartments in macrophages. *BMC Biol.* 11:89. http://dx.doi.org/10.1186/1741-7007-11-89

Moffat, J., D.A. Grueneberg, X. Yang, S.Y. Kim, A.M. Kloepfer, G. Hinkle, B. Piqani, T.M. Eisenhaure, B. Luo, J.K. Grenier, et al. 2006. A lentiviral RNAi library for human and mouse genes applied to an arrayed viral high-content screen. *Cell*. 124:1283–1298. http://dx.doi.org/10.1016/j.cell.2006.01.040

Monde, K., V. Chukkapalli, and A. Ono. 2011. Assembly and replication of HIV-1 in T cells with low levels of phosphatidylinositol-(4,5)-bisphosphate. *J. Virol.* 85:3584–3595. http://dx.doi.org/10.1128/JVI.02266-10

Nakatsu, F., J.M. Baskin, J. Chung, L.B. Tanner, G. Shui, S.Y. Lee, M. Pirruccello, M. Hao, N.T. Ingolia, M.R. Wenk, and P. De Camilli. 2012. PtdIns4P synthesis by PI4KIIIα at the plasma membrane and its impact on plasma membrane identity. *J. Cell Biol.* 199:1003–1016. http://dx.doi.org/10.1083/jcb.201206095

Naldini, L., U. Blömer, P. Gallay, D. Ory, R. Mulligan, F.H. Gage, I.M. Verma, and D. Trono. 1996. In vivo gene delivery and stable transduction of nondividing cells by a lentiviral vector. *Science*. 272:263–267. http://dx.doi.org/10.1126/science.272.5259.263

Ono, A., S.D. Ablan, S.J. Lockett, K. Nagashima, and E.O. Freed. 2004. Phosphatidylinositol (4,5) bisphosphate regulates HIV-1 Gag targeting to the plasma membrane. *Proc. Natl. Acad. Sci. USA*. 101:14889–14894. http://dx.doi.org/10.1073/pnas.0405596101

Ostrowski, M., N.B. Carmo, S. Krumeich, I. Fanget, G. Raposo, A. Savina, C.F. Moita, K. Schauer, A.N. Hume, R.P. Freitas, et al. 2010. Rab27a and Rab27b control different steps of the exosome secretion pathway. *Nat. Cell Biol.* 12:19–30: 1–13. http://dx.doi.org/10.1038/ncb2000

Pan, W., S.C. Choi, H. Wang, Y. Qin, L. Volpicelli-Daley, L. Swan, L. Lucast, C. Khoo, X. Zhang, L. Li, et al. 2008. Wnt3a-mediated formation of phosphatidylinositol 4,5-bisphosphate regulates LRP6 phosphorylation. *Science*. 321:1350–1353. http://dx.doi.org/10.1126/science.1160741

Pizarro-Cerdá, J., B. Payrastre, Y.J. Wang, E. Veiga, H.L. Yin, and P. Cossart. 2007. Type II phosphatidylinositol 4-kinases promote *Listeria* monocytogenes entry into target cells. *Cell. Microbiol.* 9:2381–2390. http://dx.doi.org/10.1111/j.1462-5822.2007.00967.x

Popovic, M., M.G. Sarngadharan, E. Read, and R.C. Gallo. 1984. Detection, isolation, and continuous production of cytopathic retroviruses (HTLV-III) from patients with AIDS and pre-AIDS. *Science*. 224:497–500. http://dx.doi.org/10.1126/science.6200935

Raposo, G., M. Moore, D. Innes, R. Leijendekker, A. Leigh-Brown, P. Benaroch, and H. Geuze. 2002. Human macrophages accumulate HIV-1 particles in MHC II compartments. *Traffic*. 3:718–729. http://dx.doi.org/10.1034/j.1600-0854.2002.31004.x

Raposo, G., M.S. Marks, and D.F. Cutler. 2007. Lysosome-related organelles: driving post-Golgi compartments into specialisation. *Curr. Opin. Cell Biol.* 19:394–401. http://dx.doi.org/10.1016/j.ceb.2007.05.001

Ruiz-Mateos, E., A. Pelchen-Matthews, M. Deneka, and M. Marsh. 2008. CD63 is not required for production of infectious human immunodeficiency virus type 1 in human macrophages. *J. Virol.* 82:4751–4761. http://dx.doi.org/10.1128/JVI.02320-07

Salazar, G., B. Craige, B.H. Wainer, J. Guo, P. De Camilli, and V. Faundez. 2005. Phosphatidylinositol-4-kinase type II alpha is a component of adaptor protein-3-derived vesicles. *Mol. Biol. Cell*. 16:3692–3704. http://dx.doi.org/10.1091/mbc.E05-01-0020

Satoh, T., and N. Manel. 2013. Gene transduction in human monocyte-derived dendritic cells using lentiviral vectors. *Methods Mol. Biol.* 960:401–409. http://dx.doi.org/10.1007/978-1-62703-218-6_30

Schindler, M., J. Münch, and F. Kirchhoff. 2005. Human immunodeficiency virus type 1 inhibits DNA damage-triggered apoptosis by a Nef-independent mechanism. *J. Virol.* 79:5489–5498. http://dx.doi.org/10.1128/JVI.79.9.5489-5498.2005

Sibarita, J.B. 2005. Deconvolution microscopy. *Adv. Biochem. Eng. Biotechnol.* 95:201–243.

Sundquist, W.I., and H.G. Kräusslich. 2012. HIV-1 assembly, budding, and maturation. *Cold Spring Harb Perspect Med*. 2:a006924. http://dx.doi.org/10.1101/cshperspect.a015420

Théry, C., M. Ostrowski, and E. Segura. 2009. Membrane vesicles as conveyors of immune responses. *Nat. Rev. Immunol.* 9:581–593. http://dx.doi.org/10.1038/nri2567

Trkola, A., M. Purtscher, T. Muster, C. Ballaun, A. Buchacher, N. Sullivan, K. Srinivasan, J. Sodroski, J.P. Moore, and H. Katinger. 1996. Human monoclonal antibody 2G12 defines a distinctive neutralization epitope on the gp120 glycoprotein of human immunodeficiency virus type 1. *J. Virol.* 70:1100–1108.

Tsuboi, T., and M. Fukuda. 2005. The C2B domain of rabphilin directly interacts with SNAP-25 and regulates the docking step of dense core vesicle exocytosis in PC12 cells. *J. Biol. Chem.* 280:39253–39259. http://dx.doi.org/10.1074/jbc.M507173200

Tsuboi, T., and M. Fukuda. 2006. The Slp4-a linker domain controls exocytosis through interaction with Munc18-1.syntaxin-1a complex. *Mol. Biol. Cell*. 17:2101–2112. http://dx.doi.org/10.1091/mbc.E05-11-1047

Várnai, P., and T. Balla. 1998. Visualization of phosphoinositides that bind pleckstrin homology domains: calcium- and agonist-induced dynamic changes and relationship to myo-[^{3}H]inositol-labeled phosphoinositide pools. *J. Cell Biol.* 143:501–510. http://dx.doi.org/10.1083/jcb.143.2.501

Vickers, J.D., R.L. Kinlough-Rathbone, and J.F. Mustard. 1982. The effect of prostaglandins E1, I2 and F2 alpha on the shape and phosphatidylinositol-4,5-bisphosphate metabolism of washed rabbit platelets. *Thromb. Res.* 28:731–740. http://dx.doi.org/10.1016/0049-3848(82)90098-6

Villalta, J.I., S. Galli, M.F. Iacaruso, V.G. Antico Arciuch, J.J. Poderoso, E.A. Jares-Erijman, and L.I. Pietrasanta. 2011. New algorithm to determine true colocalization in combination with image restoration and time-lapse confocal microscopy to MAP kinases in mitochondria. *PLoS ONE*. 6:e19031. http://dx.doi.org/10.1371/journal.pone.0019031

Wang, Y.J., J. Wang, H.Q. Sun, M. Martinez, Y.X. Sun, E. Macia, T. Kirchhausen, J.P. Albanesi, M.G. Roth, and H.L. Yin. 2003. Phosphatidylinositol 4 phosphate regulates targeting of clathrin adaptor AP-1 complexes to the Golgi. *Cell*. 114:299–310. http://dx.doi.org/10.1016/S0092-8674(03)00603-2

Wei, Y.J., H.Q. Sun, M. Yamamoto, P. Wlodarski, K. Kunii, M. Martinez, B. Barylko, J.P. Albanesi, and H.L. Yin. 2002. Type II phosphatidylinositol 4-kinase beta is a cytosolic and peripheral membrane protein that is recruited to the plasma membrane and activated by Rac-GTP. *J. Biol. Chem.* 277:46586–46593. http://dx.doi.org/10.1074/jbc.M206860200

Welsch, S., O.T. Keppler, A. Habermann, I. Allespach, J. Krijnse-Locker, and H.G. Kräusslich. 2007. HIV-1 buds predominantly at the plasma membrane of primary human macrophages. *PLoS Pathog.* 3:e36. http://dx.doi.org/10.1371/journal.ppat.0030036

Yauch, R.L., and M.E. Hemler. 2000. Specific interactions among transmembrane 4 superfamily (TM4SF) proteins and phosphoinositide 4-kinase. *Biochem. J.* 351:629–637. http://dx.doi.org/10.1042/0264-6021:3510629